João Mendonça de Azevedo

Bachelor in Materials Science

Cork as a novel material for Printed Electronics

Dissertation to obtain the degree of
Master of Science in
Materials Engineering

Adviser: Cristina Henriques Gaspar,
Senior Researcher at Almascience.

Co-Adviser: Luís Miguel Nunes Pereira,
Associate Professor at NOVA University of Lisbon.

December 2020

FACULDADE DE CIÊNCIAS E TECNOLOGIA
UNIVERSIDADE NOVA DE LISBOA

Cork as a novel material for Printed Electronics

ACKNOWLEDGEMENTS

Em primeiro lugar, quero deixar um agradecimento ao Departamento de Ciências dos Materiais da Faculdade de Ciências e Tecnologia da Universidade Nova de Lisboa por ter sido a minha segunda casa durante estes magníficos 5 anos e me ter permitido desenvolver não só a nível académico, mas também pessoal. Levo comigo recordações e saudade para a vida.

Obrigado aos meus orientadores, Dra. Cristina Gaspar e Professor Luís Pereira, por toda a ajuda em momentos chave deste trabalho bem como pela total abertura para discutir ideias que tiveram comigo.

Um agradecimento ao Professor Rodrigo Martins e à Professora Elvira Fortunato por toda a dedicação e trabalho inovador que têm desenvolvido, concedendo as condições ideais para a investigação científica no CEMOP e CENIMAT.

O meu sincero obrigado a todo o grupo de trabalho do CEMOP e do CENIMAT, que me acolheram da melhor maneira desde o primeiro dia e proporcionaram um excelente ambiente para desenvolver a minha tese. Em especial, o meu muito obrigado à Inês Cunha, Diana Gaspar e Joana Figueira por toda a disponibilidade e muita paciência que sempre tiveram comigo. Sem a vossa ajuda, tudo teria sido muito mais difícil de realizar.

À minha família, e em especial à minha Mãe, por me terem fornecido sempre as melhores bases possíveis para que pudesse ser tudo o que sou hoje. À minha Avó Arminda e ao meu Avô Zé, por terem sido o melhor porto de abrigo que tive desde que me lembro de existir. Obrigado por me terem educado com os mais belos valores de vida e me mostrarem que tudo é possível. Mais cedo ou mais tarde, voltaremos a estar juntos.

A todos os meus amigos que sempre estiveram presentes em todos os momentos da minha vida e sempre me deram conselhos valiosos ao longo do tempo. Obrigado por todas memórias únicas que criamos e continuamos a criar.

ABSTRACT

Cork is one of the oldest materials used by Man, with exceptional characteristics that allow its introduction in the field of electronics as a material that is not only innovative but also sustainable. Composite cork agglomerates from cork industrial waste have all the intrinsic properties of natural cork, making it a great starting point for introducing cork into electronics. Motivated by the growing need in the use of new natural and self-sustainable materials, it was developed with the use of another ecological and innovative material, cellulose nanofibers, a simple, low energy and low-cost method of surface planarization, which improves significantly the surface characteristics of cork for later use as an electronic substrate.

Several surface studies were carried out on the cork agglomerate at various stages of the planarization process to optimize each step of the overall process. Due to the hydrophobicity of cork surface, oxygen low-pressure plasma treatment was performed as an essential initial step for surface activation, followed by an extensive surface analysis through SEM, ATR-FTIR spectrum, contact angle measurements, and surface energy calculation to understand the induced changes. Subsequently, several types of thin cellulose nanofibers layers were applied over the activated cork agglomerate surface, significantly reducing the surface roughness hitherto presented, with improved adhesion. As a result, planarized cork agglomerate substrates display lower surface roughness, being optimized to be used in a wide range of electronic devices.

Proving its applicability in electronic devices, the produced planarized substrates were successfully used alongside carboxymethyl cellulose and zinc oxide in the development of screen-printed ultraviolet sensors, presenting high production replicability, higher photocurrents than the equivalent substrate without any type of treatment, and stable performances over continuous use cycles.

Keywords: Cork, cork electronics, printed electronics, cellulose nanofibers, planarizing layer, ultraviolet sensors.

RESUMO

A cortiça é um dos materiais mais antigos utilizados pelo Homem, com características excecionais que possibilitam a sua introdução no campo da eletrónica como um material não só inovador, mas também totalmente sustentável. Aglomerados compósitos de cortiça provenientes do desperdício industrial apresentam todas as propriedades intrínsecas da cortiça natural, sendo assim um ótimo ponto de partida para a introdução da cortiça na eletrónica. Motivado pela crescente necessidade que a indústria eletrónica apresenta na utilização de novos materiais naturais e autossustentáveis, foi desenvolvido com a utilização de outro material ecológico e inovador, as nanofibras de celulose, um método de planarização superficial simples e de baixo custo energético, que melhora de forma significativa as características superficiais da cortiça para posterior utilização como substrato eletrónico.

Em primeiro lugar, foram realizados diversos estudos superficiais ao aglomerado de cortiça em várias etapas do processo de planarização, a fim de aperfeiçoar cada passo do processo global. Devido à hidrofobia da cortiça, foi realizado como etapa inicial do processo um tratamento de plasma a baixa pressão com oxigénio essencial para a ativação superficial, juntamente com uma extensa análise superficial através de SEM, espectro ATR-FTIR, medição do ângulo de contato e cálculo da energia superficial de modo a analisar as alterações provocadas. Posteriormente, diversos tipos de camadas finas de nanofibras de celulose foram aplicadas sobre a superfície ativada da cortiça, diminuindo de forma acentuada a rugosidade superficial até então apresentada. Como resultado, foram obtidos substratos planarizados que apresentam rugosidades muito inferiores às iniciais, estando otimizados para utilização num vasto leque de dispositivos eletrónicos.

Comprovando a sua aplicabilidade num dispositivo eletrónico, os substratos planarizados foram utilizados com sucesso na criação, através de screen-printing, de sensores ultravioleta de carboximetilcelulose e óxido de zinco. Estes sensores possuem elevada reprodutibilidade de produção, fotocorrentes superiores ao substrato equivalente sem qualquer tipo de tratamento e performances estáveis ao longo de ciclos contínuos de utilização.

Palavras-chave: Cortiça, eletrónica em cortiça, eletrónica impressa, nanofibras de celulose, camada planarizadora, sensores ultravioleta.

TABLE OF CONTENTS

LIST OF FIGURES

LIST OF TABLES

ACRONYMS

0.60CNF – 0.60wt. % CNF

0.75CNF – 0.75wt. % CNF

0.95CNF – 0.95wt. % CNF

TEMPO – 2,2,6,6-tetramethylpiperidine-1-oxyl radical

a.u. – Arbitrary units

ATR-FTIR – Attenuated Total Reflectance - Fourier Transform Infrared Spectroscopy

CMC – Carboxymethyl cellulose

CNF – Cellulose nanofibers

CENIMAT|i3N – Centro de Investigação de Materiais | Instituto de Nanoestruturas, Nanomodelação e Nanofabricação

LPPT – Low-pressure plasma treatment

RH – Relative humidity

SEM – Scanning Electron Microscopy

UV – Ultraviolet

wt. – Weight ratio

LIST OF SYMBOLS

$\boldsymbol{\gamma_D}$ – Dispersion forces

$\boldsymbol{\gamma_{ND}}$ – Non-dispersion forces

$\mathbf{I_{dark}}$ – Dark current

$\mathbf{I_{light}}$ – Photocurrent under UV illumination

$\mathbf{I_{ph}}$ – Photoresponse current

P – Power

$\boldsymbol{p}$ – Pressure

$\mathbf{p_s}$ – Photosensitivity

$\boldsymbol{p_w}$ – Working pressure

T – Time

$\mathbf{t_{fall}}$ – Fall time

$\mathbf{t_{rise}}$ – Rise time

$\mathbf{W_A}$ – Work of adhesion

$\boldsymbol{\gamma}$ – Surface energy

1. MOTIVATION

Looking at the World today and to us, Humans, it is easy to perceive that our dependence on technology in our daily lives is huge. Imagining a single day without the use of an electronic device, no matter how simple the device, is practically an impossible task. Feeding this dependence on technology, an ongoing technological revolution is providing us with new types of electronic devices, creating more and more functionality in these devices and, in a way, end up influencing our simple existence progressively. [1] We can state that small electronic devices and the "Internet of Things" are revolutionizing our society. However, this revolution is not being done sustainably. This electronic development is based on materials such as high-grade silicon, metals, or both materials and the process of how we obtain them (mining) and process them still requires high energy expenditure. Altogether are harmful to the environment and their use must be rethought. Also, electronic devices, considered most often as disposable, are made up of toxic metals and organics, difficult to recycle, and are not biodegradable. Therefore, the problem of electronic waste is growing nowadays, presenting itself as a threat to public health and the environment. [2] Aside from all these problems, unease related to the availability of the so-called "critical materials", the ones essential to the production of electronic devices, became real to the society when in 2010, the world market was disturbed by the fact that the demands of the world's electronic industries could not be met by the available supplies, thus creating the need for new alternatives. [3]

Printed Electronics can be the key factor in a "new wave" of sustainable electronic development. Unlike conventional electronics, they present themselves as a sustainable alternative due to the use of environmentally friendly and Earth-abundant materials. In addition to this, it is endowed with high energy efficiency, thus not requiring complex and expensive processes for manufacturing the electronic devices, characterizing it as low cost. Furthermore, some of these printed devices may even be recycled later. [4]

Printed electronics are also innovative in terms of flexibility. There is an increasing interest from both industry and consumers in flexible electronic devices, largely because of the exceptional properties they offer: lightweight, bendable, conformable, rugged, and not easily breakable. Therefore, the wide range of applications possible to be printed on flexible substrates are capable of being molded or bent, unlike silicon electronics. [5,6]

The cork industry plays an important socio-economic role in the countries of the western Mediterranean. In the Portuguese case, the importance is even greater since is the world leader in the production and processing of cork. However, this industry creates a considerable value of material waste, with cork powder being the main waste of the cork industry (approximately 30.000 tons/year). [7] To reduce this waste, new applications for cork waste material are being considered. Cork composites display themselves as one of the most promising fields of cork technology evolution, as cork properties present in natural cork are also present in them. [8]

2. OBJECTIVES

Understanding the necessity of creating a sustainable green future in the topic of electronics, this master thesis will combine the use of abundant organic materials allied with low-cost, energy-efficient processes to create first a planarized substrate and secondly, a screen printed ultraviolet (UV) sensor on the optimized planarized substrate. Cellulose-based substrates, such as paper or cork, have been in the spotlight of research and development at *Centro de Investigação de Materiais/Instituto de Nanoestruturas, Nanomodelação e Nanofabricação* (CENIMAT|i3N), leading to a vast work done on the topic of cellulose as a major component in printed electronics.

Using cork agglomerate composites as a groundbreaking substrate, this thesis reports the creation of a cellulose-based planarization layer, that will provide a pioneer contribution to a new perception and knowledge of revolutionary printed electronics based on cork material. Simultaneously, several characterization techniques will be employed to understand deeply how the different steps of this work change/improve the cork agglomerate surface towards its planarization. Also, the created planarized substrates will have as proof of concept a successful assembly of a screen-printed UV sensor on them.

3. INTRODUCTION

For a complete understanding of this master's thesis, an introduction to the most prominent topics will be made in this chapter. Beginning with a global analysis of the material under study, cork, going on to fundamentals and explanations about the main topics of interest, such as printed electronics and its printing techniques, UV sensors, a planarization layer, and cellulose nanofibers.

3.1. Cork: raw material and characteristics

Cork is a timeless material, used by mankind since Ancient History until the present day. [9] It performs a considerable role in the social and economic development of the Western Mediterranean countries, in which Portugal is included. Portugal has a special connection with this material, holding a substantial cork oak forest inside its borders (737000 hectares, 34% worldwide) [10] and being the world leader in cork production, controlling about 50% of the total global market, which is equivalent to 100000 tons. [11] Also, Portugal is by far the biggest World exporter of cork products, owning 63% of the world trades and generating an income of 986.3 million euros, as reported by Banco de Portugal in 2016 and updated in 2018. The cork industry in the Mediterranean countries is estimated to employ about 100000 workers and in Portugal's specific case, about 8310 workers. [11] From an ecological point of view cork also presents itself as a very interesting material, considered a sustainable material. Cork oak forests prevent desertification and keep a close role in the maintenance of biodiversity. [12] Furthermore, cork is harvested without the demand of killing the tree, granting that is possible to extract bark from that same tree in the future and harvested oaks absorb 4 times more carbon dioxide than unharvested ones. [8,11]

The *Quercus Suber L.* cork microscopic morphology is characterized by layers of homogeneous thin-walled cells that are organized without any kind of intercellular space, creating an alveolar structure, and offering cork a hollow honeycomb microstructure, as Figure 1 shows. Chemically speaking, cork is constituted predominantly by suberin (40%), lignin (22%), polysaccharides (18%), and extractables (15%). [13,14] Physical properties of *Quercus Suber L.* cork are extraordinarily fascinating. This material accommodates a combination of insulation properties, low density, lightness, elasticity, gas and water impermeability, surface and dielectric properties as well as being fire retardant. [13,15] Giving an insight towards the surface properties, cork is a hydrophobic material with low wettability towards polar liquids and high affinity for non-polar, with a surface energy of 18 mN m^{-1} and the contact angle of water on cork is between 84 º and 100 º. [16]

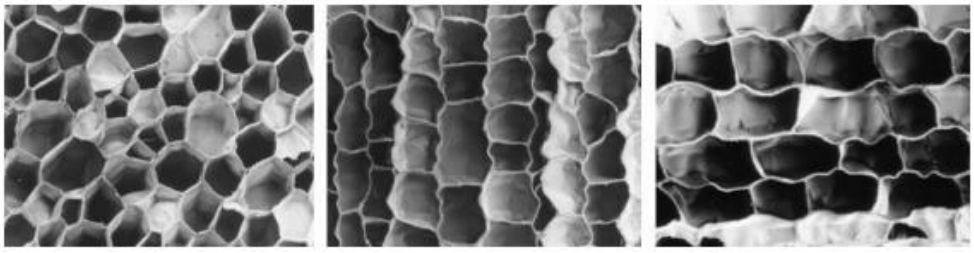

a) Tangential section **b) Transverse section** **c) Radial section**

Figure 1 – SEM images of the three sections of cork: a) tangential, b) transverse and c) radial. Adapted from [16] with no scale bar available.

Besides traditional applications such as a wine stopper or a naturally insulating material, cork can also be used to produce agglomerates. Since large amounts of cork are discarded during the production of stoppers, wasted material is granulated, mixed with a polymeric binder, and compressed under heat and pressure. Size and fraction of cork granules in the mixture, type of polymeric binder, and packing density are the main variables to consider during the production of cork agglomerates, depending on the use that will be given after to the agglomerates. Innovation starts to flourish on the use of cork in new ways, thanks to its remarkable characteristics. [13]

3.2. Cork as a new substrate in printed electronics

We live in a world that is progressively more dependent on electronic devices, verified by the rising of connected devices each year [17]. Consequently, electronic waste is a growing problem to be solved, suggesting a need for sustainable and eco-friendly materials. [17,18] Considering the previously mentioned properties, cork starts to be recognized as a material that can be used in technological evolution by a wide range of professionals. [19] Corroborating that, published works [17,20,47] focused on cork are increasing with time, showing a flourishing interest of the scientific community on this material.

For example, fully printed UV sensors on a cork substrate have been created for the first time at CENIMAT|i3N, proving that is possible to use this material as an alternative low-cost and sustainable substrate for printed electronics. [17] Radio-Frequency Identification tags also have been created using pressed cork agglomerates, given its isotropic behavior, as they display excellent characteristics such as low permittivity, roughly the same loss tangent values over the whole directions of the material, and a low dissipation factor. The work done by Gonçalves et al. shown good results and proven that the material can be used for this type of device. Also, a passive humidity sensor could be created using cork as the sensing surface since cork is a porous dielectric material and therefore, absorbs water. This characteristic enables sensitivity to humidity changes. [20]

3.3. Printed electronics and printing techniques

The production of traditional electronic devices requires the use of vacuum and high temperatures, corrosive chemicals, expensive sophisticated equipment, and large infrastructures, creating huge energy consumption and complexity of processes. [13] In addition to a vast interest in the use of eco-friendly materials, the use of sustainable processes from an environmental and financial point of view is also becoming increasingly vital today. Printing techniques have received great prominence as they can comply with the requirements of sustainability due to their distinctive characteristics: simplicity, high adaptability, cost-effectiveness, and adaptability to the fabrication process, as well as being suitable to use with eco-friendly materials, culminating in the production of eco-sustainable devices. [17,19,21] Therefore, printed electronics are an innovative technology that allows us to create a wide range of devices such as sensors and transistors, for example, on low-cost and flexible substrates. [12]

Targeting the best properties possible for a specific device, the chosen printing method should not be trivial. To achieve very high-definition patterns, we should think about using a technique that provides a very small line width and thickness such as nanoimprint, with the

downside of the slow speed. However, focusing on fast printing, techniques such as offset, and gravure printing should be used because of its high throughput speed. Thinking about straightforward and economical techniques, inkjet and screen-printing, firstly they grant precise patterning with reduced raw material waste and secondly having as best features simplicity, adaptability, and reliability even when performed manually on an affordable and homemade system. [22] Thus, in a wide range of available printing techniques, screen-printing stands as the most mature of them all, given its simplicity and reproduction. [23]

The manual screen-printing system can be described as flat support incorporating a previously patronized screen inside its frame, holding it, and giving stability to the whole system. Ink is pushed through a patterned screen with a squeegee, leaving the pattern printed on the substrate, as shown in Figure 2. High-speed screen-printing tools own a commercial resolution worse than 50μm. Therefore, to obtain the optimal performance of this technique, several parameters related to the screen mesh properties, intrinsic ink characteristics, printing speed, and external factors embracing the operator should be considered. Aiming attention at the ink, parameters such as viscosity, surface tension, wettability, and adhesion to the substrate should be fine-tuned, with the use of high viscosity inks or pastes being mandatory as they prevent excessive spreading and bleed-out through the used mesh. On the other hand, binders used to make the ink viscous create a loss of performance. [22-24] The viscosities used in screen-printing are relatively high, with values usually over 1000 cP. High viscosity is required to prevent excessive spreading and bleed-out during the printing. [24]

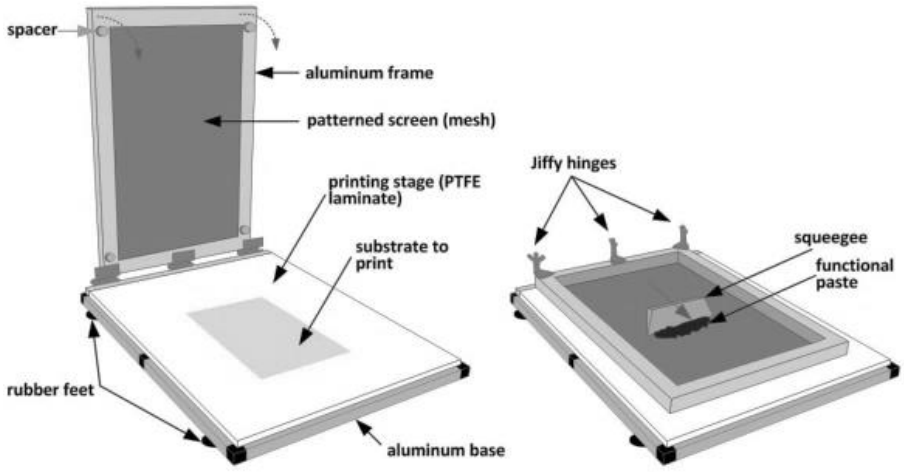

Figure 2 – Schematic drawing of custom-made manual screen-printing system used at CENIMAT|i3N. Adapted from [22].

In summary, parameters such as viscosity, solvent compatibility, physical and chemical stability, and surface energy compatibility alongside resolution limits of printing techniques already referred tend to negatively influence the performance of the printed devices. [23]

3.4. New perspectives for cork in printed electronics

Although cork can play a fundamental role in the production of “green” electronic devices, there are few reports on using cork as a substrate for printed electronics. Therefore, among other devices, UV sensors integrated into cork substrates could start to introduce cork as a new “green” material to be used in the growing market for smart and wearable products. [17]

To understand the potential of cork as a substrate for a UV sensor, an insight into the fundamentals of UV sensors is going to be explained below, allied with a brief introduction to zinc oxide (ZnO) main characteristics and application in electronics devices.

There is a growing appeal to the synthesis and application of nanoscale materials, in the field of electronic devices. These nanoscale materials present exclusive mechanical, electrical, optical, and chemical properties that are different from the bulk, mainly because of their high surface-to-volume ratio and spatial confinement. [25,26] Materials such as ZnO feature a wide bandgap of 3.34 eV and a large exciton binding energy of 60 meV at room temperature, thus ZnO is transparent to visible light. It has a semiconductor behavior, meaning that can be made highly n-type conductive by doping. ZnO nanostructures have a high specific surface area, low toxicity, chemical stability, electrochemical activity, and high conductivity, opening the door to its use in high-performance sensors. [27] Therefore, ZnO stands out as one of the most important metal oxides due to its exclusive properties alongside a high transmittance in the visible region and a high chemical, thermal, and mechanical stability. To achieve the optimal electrical and optical properties of ZnO films, the deposition conditions, type of substrate, temperature, oxygen (O_2) partial pressure during the deposition, and the final film thickness should be taken into consideration. [28, 29] There is an attempt to develop different ZnO nanostructures with improved properties since the shape and aspect ratio of the nanostructure are fundamental parameters to reach better electrical and optical properties. [30] Various morphologies and dimensions for ZnO have been synthesized so far, granting the possibility of the use of diverse nanostructures such as nanorods, nanotubes, nanocorals, nanoflower, and nanowalls [29]. Also, ZnO is a recognized UV-radiation-photosensitive material given its standard proprieties, allowing its use at UV sensors. [17] Boosting all these exceptional features, ZnO is also low-cost, biocompatible, and eco-friendly [18].

Before explaining the fundamentals of a UV sensor, a brief insight into UV light is essential. UV light can be characterized as electromagnetic radiation owning a wavelength between 10 nm (124 eV) and 400 nm (3 eV) and has four divided spectral regions, with most of the UV light emitted by the Sun being absorbed by the atmospheric ozone layer. [27]

Firstly, UV sensors have been used in extraterrestrial applications, however over time, terrestrial applications have also been discovered for them. Chemical, environmental, and biological analysis or monitoring, flame and radiation detection, astronomical studies, and optical communications stand as examples of how the detection of UV radiation can be used. Focusing on the modern-day semiconductor photodetectors, they present us a great sensitivity, great stability of response, and provide good linearity characteristics. The working principle of most of these UV sensors is the internal photoelectric effect in which an electron-hole pair is created due to the excitation of an electron from the valence band to the conduction band, provided by the absorption of a photon by the semiconductor. Providing an electric field, the movement of the free charges starts and creates a current in the detector. [31] Figure A.1 – Annex A displays a scheme that represents the working principle of the UV sensors.

To have a high-performance photodetector, high sensitivity, high signal-to-noise ratio, high spectral selectivity, high speed, and high stability should be assured. One-dimensional nanostructures, such as ZnO UV sensors, must be considered as they show improved sensitivity to light due to their large surface-to-volume ratio and Debye length comparable to their small size, providing enhanced photosensitivity. [27] Testifying that, over the last two decades the

research over one-dimensional nanostructures has increasing interest over the scientific community, especially due to their outstanding properties and potential applications. [28]

3.5. Planarization layer

With the expected market growth of the printed electronic devices combined with many of them being disposable, there is also a growing need for the use of biodegradable materials as a substrate, contrasting with the present-day solution of using plastic. [32] Paper, for example, is being employed as a flexible substrate material for printed electronics because of wide availability, low-cost, and being environmentally friendly. [33]

However, these biodegradable materials might not have the suitable requirements to be used as-is in the production of printed electronics since, for example, the roughness and porosity of paper are typically high and their chemical, mechanical and thermal stability is worse than the ones of plastics, leading to a negative influence over the device stability. Despite being possible to improve the gas and chemical barrier properties of paper, the rough surface remains a problem when printing conductive lines on this material. [32-34]

3.5.1. Oxygen plasma treatment

Plasma, also called the fourth state of matter, can be defined as an ionized gas and its constituent of more than 99% of the universe. It is composed of a set of atoms in excited states, free radicals, metastable particles, electrons, and ions and although from a macroscopic point of view plasma is electrically neutral, it contains free charge carriers and electrical conductivity. At a laboratory scale, low-pressure plasma is created by applying electrical energy to a previously selected gas. The electric field starts to excite the gas electrons, generating electronic energy that is transmitted to neutral species through collisions. Most of the excited species then release a photon and return to a neutral state in a very short space of time. There are several types of surface treatments that can be performed using plasma: cleaning (decontamination and grease removal), activation (adherence or anti-adherence properties), etching, and functionalization (electrical conductivity, protection against corrosion, and chemical barrier), among others. [35,36] A scheme of plasma instrumentation can be seen in Figure A.2 – Annex A. Enhancement of surface reactivity and wettability are some of the advantages that are obtained when using this type of surface treatment. In the case of surface activation, using the example of an argon-oxygen plasma treatment, polar and hydrophilic functions are propagated through the surface of the material under treatment which translates into an increase of the material surface energy. This kind of activation is useful to prepare the surface before other treatments such as printing and coating, as it increases wettability and promotes adhesion, for instance. [36]

Cork is a hydrophobic material due to the biopolymer suberin and therefore low adhesion between cork surface and other materials is expected. [35] The use of surface chemical treatments towards a change in the surface properties of different materials has shown some success in increasing the capacity of interfacial bonding. However, the high cost of these treatments, the disposal of chemical products used, and the environmental pollution associated with them narrow their industrial application. Differently, plasma treatments are considered a clean dry process with huge environmental potential and energy conservation benefits, modifying the surface of several materials without affecting its intrinsic properties. [38] Thus, giving the cork surface a plasma treatment will generate a change in hydrophobicity towards a more compliant surface to coatings.

In comparison to polymers, plasma treatments modify the wettability of the cork surface, allowing subsequently to spread a layer of another material on an adhesive form on the surface without changing the intrinsic characteristics of the cork. [35]

In this work, surface activation through an O_2 low-pressure plasma treatment (LPPT) is the necessary step to be made to achieve a hydrophilic surface. [35] Since low pressure is used, the treatment can be carried out at low or moderate temperatures. Because of this, the aggressiveness of the plasma treatment is reduced, hence low degradability of the material under treatment is guaranteed. [39] LPPT can deliver a large variety of surface modifications allied with a positive environmental and economical aspect, increasing the general interest in the use of this technique to achieve desired surface modifications. [40] Silva et al. presented a study of how plasma treatment can affect the surface, wettability, morphology, and chemical composition of cork agglomerate. In conclusion, the study proved that plasma treatment can create more polar groups, increase surface energy, improve wettability, and increase the work of adhesion of the samples. Also, it is shown that plasma treatment can change the surface of cork agglomerates without changing their bulk characteristics. [47]

3.5.2. Cellulose nanofibers

Cork surface has well known discontinuities that influence the in-use performance of cork products. Heterogeneity of the cork surface exists due to the presence of lenticular channels, woody inclusions, small fractures, and other defects referred to as porosity of cork. [34] To overcome such problems associated with the roughness of the surface in organic devices, a planarization layer should be applied. This layer will play an important role both in terms of the device's performance as well as its reliability. We can consider that this layer serves multi-purposes such as smoothing the substrate surface for device fabrication, creating better adhesion of organic materials on the substrate, improved wetting for organic semiconductors, and stable electrical performances. [41]

Cellulose nanofibers (CNF) are a nanomaterial with a bio-based origin, widely available, renewable, non-toxic, biodegradable, and simultaneously owning outstanding properties that can be used as a coating layer in printed electronics applications. [42] CNF has a high aspect ratio, high specific strength, flexibility, large specific surface area, and thermal stability, combined with biodegradability and biocompatibility. At a structural level, CNF can be compared to a “spaghetti”-like structure and can be obtained through their isolation from wood and plant cell walls, using chemical, enzymatic, and/or mechanical treatments. [42,43] However, the mentioned processes generally require a high number of passes and therefore, high energy consumption. Pre-treatment methods, an enzymatic treatment, can facilitate the fibrillation of cellulose fibers and decrease energy consumption. CNF display their diameter in the nanometer range and length dimension in the microns scale, depending on the processing and pre-treatment methods. The combination of all these exceptional features (structure, mechanical properties, and surface reactive chemistry allows CNF to be used in a wide range of applications. [44]

The work of Hamada et al. shows how the coating of synthetic fiber sheets with CNF provokes changes at the level of the surface roughness and contact angle (alongside with other properties) of the coated sheets, providing excellent insights on how CNF can cause an increase in ink density and print quality. Also, this shows that CNF can be incorporated as a low-cost surface treatment in the form of a coating that creates porous hydrophilic surfaces. [45]

4. MATERIALS AND METHODS

In this chapter, all the necessary steps along the process of creating a CNF coating layer, and its further characterization will be described. Furthermore, the production and posterior characterization of screen-printed UV sensors on cork agglomerate CNF planarized substrates will be also described.

4.1 Cork agglomerate

The access to the used cork agglomerate in this work was made through a local shop, where cork agglomerate strips measuring 2 m width and 6 cm wide from the brand "Eva Arte" reference "83263" were obtained. Afterward, the raw cork agglomerate strip was cut using scissors to create rectangular-shaped samples with dimensions of 6 cm wide and 5 cm width, facilitating all the necessary subsequent steps of the process. Neither solvent wash nor any other kind of pre-treatment was made before the cut of cork agglomerate samples.

4.2. Oxygen low-pressure plasma treatment

The O_2 LPPT was performed with an LPPT system from the Diener Electronics ZEPTO model. This system allows total control of the following experimental variables: pressure (*p)* of the vacuum chamber from 0.1 to 1 mBar, generator power (P) from 0 to 100 W, O_2 gas supply mass flow, working pressure (p_w) of the vacuum chamber from 0.1 to 1 mBar and time (T) of plasma treatment. Table B.1 – Annex B resumes all four plasma treatments performed to cork agglomerate samples and their respective nomenclatures.

4.3. Cellulose nanofibers mixtures formulation and application

The bulk CNF mixture used at this work has a weight ratio (wt.) of 0.95% CNF in deionized water and was obtained with commercial bleached sulphite eucalypt pulp that went through a pre-treatment with 2,2,6,6-tetramethylpiperidine-1-oxyl radical (TEMPO) – mediated oxidation and mechanical treatment. Scanning Electron Microscopy (SEM) image of some fibrils of this CNF mixture can be seen in Figure B.1 – Annex B. Attenuated Total Reflectance - Fourier Transform Infrared Spectroscopy (ATR-FTIR) was performed to characterize the spectrum of the CNF, with the results from this analysis shown in Figure B.2 – Annex B.

At this work, three CNF solutions with different wt. were used. The first solution uses the bulk CNF mixture of 0.95wt. % CNF (0.95CNF) in deionized water, while for the formulation of the other 2 solutions the bulk mixture was diluted to a weight ratio of 0.75wt. % (0.75CNF) and 0.60wt. % CNF (0.60CNF), respectively in deionized water. Before the next step, the three solutions were stirred using a magnetic stirrer at room temperature for 1 hour each for homogenization.

To coat the samples, an auto bar coater system from RK Printcoat Instruments, model K Control Coater 101 equipped with a close wound meter bar was used. Two types of bars were used, one with a 0.51 mm wire diameter and a wet film deposit of 40 μm and another with a 1 mm wire diameter and wet film deposit of 80 μm. This auto bar coater allows the control of the coating speed between 2 and 15 m min^{-1}. Table B.2 – Annex B resumes all the 12 CNF planarized cork agglomerate samples produced by the auto bar coating system and their respective nomenclatures. Another planarization method was also applied at this work, using a membrane

created with the bulk CNF solution. This membrane was laminated through a simple process to the surface of one formerly CNF coated sample, creating sample 0.95CNF-M.

4.4. UV sensor production and characterization

The screen-printing technique, as shown in Figure 2, was used to produce the UV sensors. Adapted from Figueira et al. [17], the composite semiconductor ink was a mixture of ZnO and carboxymethyl cellulose (CMC, CAS:9004-32-4, Aldrich). The ink content was 40wt. % ZnO nanopowder (<100nm, CAS:1314-13-2, Aldrich) and 3wt. % CMC in deionized water, with a weight ratio of 40:60 respectively. The commercial conducting carbon ink used to print the interdigital electrodes on top of the semiconductor layer was CRSN2644 from Sun Chemical.

For the comparison between the glass and planarized cork substrates, laboratory glass from Marienfeld with 1 mm thickness was used. Before the screen-printing of the UV sensors, the glass underwent a UV-irradiation surface treatment for 30 minutes using a UV-ozone cleaner from Novascan PSD Series. An Agilent 4155C semiconductor parameter analyzer connected to an Everbeing probe station equipped with a Thorlabs 365 nm wavelength UV light regulated by a Sanworks Pulse Pal was used to electrically characterize and evaluate the performance of the UV sensors.

4.5. Characterization methods

4.5.1. Contact angle and surface energy

Static contact angle and surface energy (γ) of all samples produced during this work were obtained through a Dataphysics OCA15 Plus system. For each sample, three measurements were done through the sessile drop technique on 3 different spots. After the measurement, the measured static contact angles were used to calculate the work of adhesion of the samples.

To attain the surface energy dispersive and polar components values using the Wu method, four liquids with known surface energy components were used. Surface energy components of the four used liquids (deionized water, glycerol, ethylene glycol, and diethylene glycol) are presented in Table B.3 – Annex B. [48,50]

4.5.2. Scanning electronic microscopy

SEM was used to observe and analyze the surface morphology of untreated, LPPT treated and LPPT treated CNF coated cork agglomerate samples produced. The results displayed in this work were obtained using a Zeiss AURIGA CrossBeam and Hitachi TM 3030Plus Tabletop system. ImageJ software was used to perform measurements on the obtained SEM images.

4.5.3 Attenuated total reflectance - Fourier transform infrared spectroscopy

ATR-FTIR was used to gather the spectrum of different samples produced in this work. All the results were obtained using a spectrometer device from Thermo Electron Corporation Nicolet 6700, using a SMART iTR adapter. The spectrums were collected at room temperature using a 4500-525 cm^{-1} range, with 32 scans allied to a spectral resolution of 4 cm^{-1}.

5. RESULTS AND DISCUSSION

In this chapter, the main results obtained throughout this work will be shown and analyzed. First, the effect of LPPT on the cork agglomerates will be analyzed, with a special focus on its morphological and surface characteristics, to optimize the LPPT for the following CNF coating. Then, an analysis of the surface properties of the CNF coating applied after the LPPT to the cork agglomerate was also performed, to optimize this coating treatment. Finally, a fully optimized CNF coated cork agglomerate was used as a substrate in the production of a UV sensor, and the results of its electrical characterization were compared with a UV sensor produced without any substrate treatment.

5.1. Production and characterization of a planarized cork agglomerate substrate

Samples were treated under LPPT with four different times of plasma treatment. The time increase in the plasma treatment was done to evaluate the possible changes in morphology and superficial characteristics of the cork agglomerate due to the LPPT. The pressure of the vacuum chamber, generator frequency power, O_2 gas supply mass flow and working pressure of the vacuum chamber was maintained the same in the production of all samples.

Cork agglomerate samples were placed on a glass holder inside the system chamber and low pressure was created inside the chamber using an external vacuum pump. After the pressure reached approximately 0.15 mBar, 17 standard cm^3 min^{-1} of O_2 was fed into the chamber via a gas flow control system until the pressure reached its working value of 0.3 mBar. Then, the generator was switched on, O_2 started to get ionized and consequently, the sample was exposed to plasma. At the end of the plasma treatment, the samples were taken out of the chamber and stored at room temperature with approximately 50% relative humidity (RH) until testing and coating with CNF.

SEM images shown in Figure 3 verify the general surface heterogeneity of the cork agglomerate, with areas of high compression of the cellular structure and the presence of several surface defects of different sizes and depths. All these surface defects in the cork agglomerate cause this substrate to have a high roughness, negatively influencing the manufacturing of any type of electronic device. [32-34] Additionally, it is possible to see the layer composition of the cork agglomerate with the cork granules bonded together over a layer of cloth material.

Comparing higher magnification SEM images from the untreated sample and from the one that underwent the longest plasma treatment time, the honeycomb structure of the cork agglomerate stays conserved but underwent slight changes in the size of the structural cells. Structural cells look less compressed and slightly rounder than the ones from the untreated sample, which leads to these having a slightly larger cell size and thinner cell walls. These results are in line with what was observed in the work of Abenojar et al. [35]

Additionally, it is possible to see the layer composition of the cork agglomerate. The cork granules are bonded together and fixed over a layer of fabric material as the cross-section SEM Figure 4 shows. To obtain the average thickness of the untreated cork agglomerate, a micrometer was used. The measured thickness value was approximately 0.46 ± 0.11 mm.

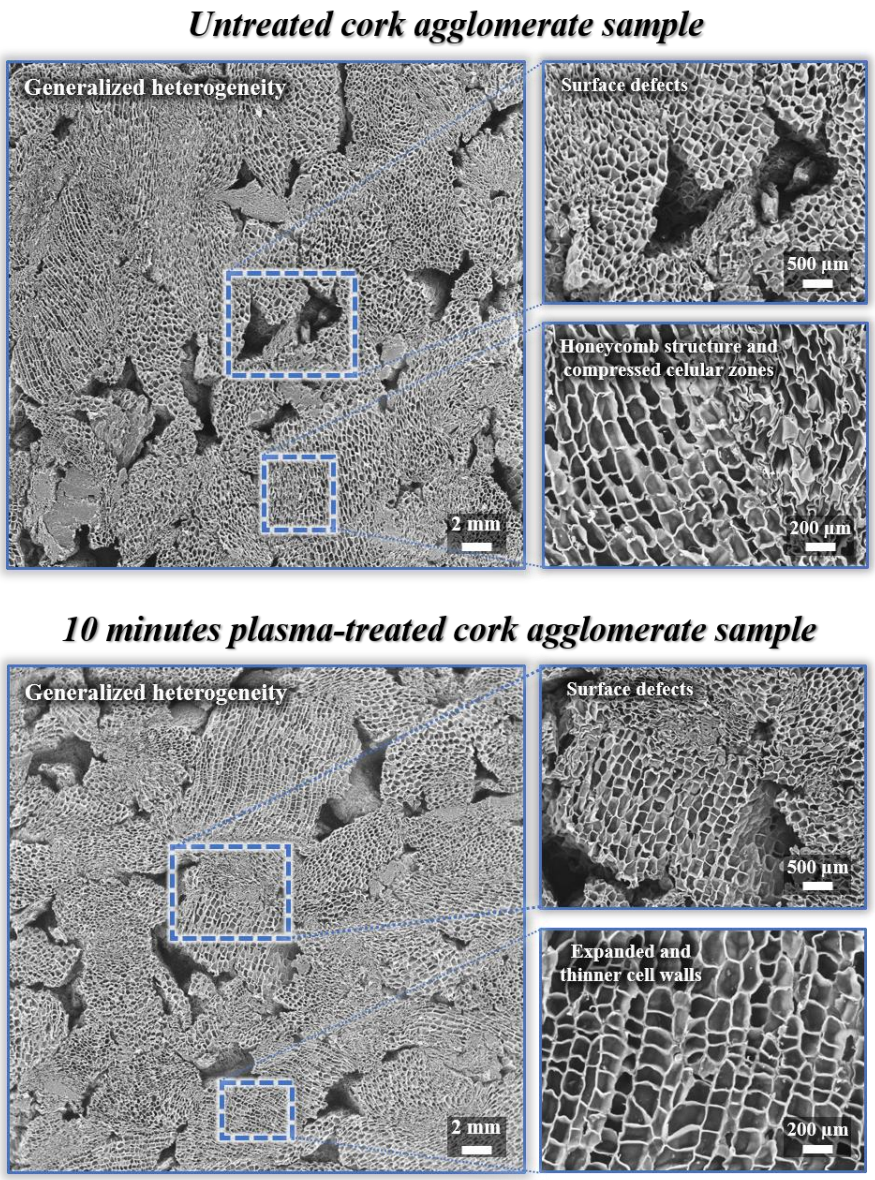

Figure 3 – SEM images of untreated and 10 minutes plasma treated cork agglomerate samples showing general surface heterogeneity and noteworthy details of the honeycomb structure.

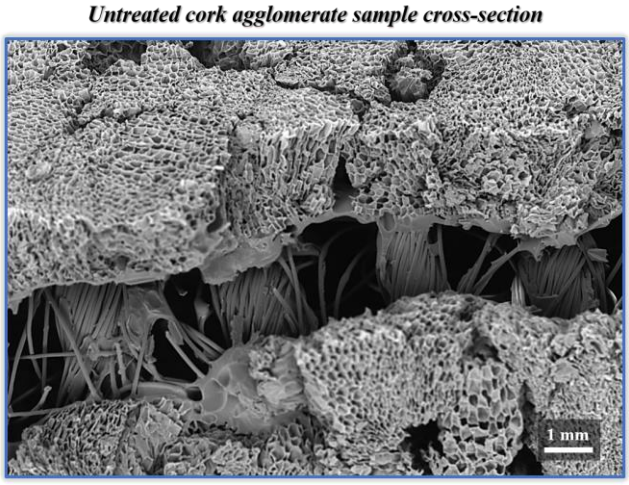

Figure 4 – SEM image of untreated cork agglomerate cross-section.

Cork exhibits a complex FTIR spectrum with many peaks and bands, due to its chemical composition. This complexity is caused by the coupling of vibrations, named skeletal vibrations, over a large part or all the molecules, creating fingerprint signals of the molecules and not of the functional groups. [35] ATIR-FTIR spectrum from the untreated cork sample and the sample that underwent the maximum time of LPPT, 10 minutes, were analyzed and compared to detect possible superficial chemical modifications due to LPPT.

In Figure 5 it is possible to notice noteworthy cork FTIR absorption details such as the 2917 cm^{-1} and 2850 cm^{-1} peaks related to suberin, the characteristic fingerprint region related to hemicelluloses and lignin at 1800-600 cm^{-1}, respectively, where: lignin is marked by 1510 cm^{-1}, 854 cm^{-1}, and 817 cm^{-1} bands, polysaccharides are represented at 1093 cm^{-1} band and extractives are represented by the 1600 cm^{-1} and 1460-1300 cm^{-1} bands. Accordingly, the FTIR spectrum of the 10 minutes plasma-treated sample shows no significant structural chemical changes compared to the untreated sample FTIR spectrum, ensuring that plasma treatment does not modify the chemical structure of the cork agglomerate. Further, higher absorbance peaks in the plasma-treated sample at 1364 cm^{-1} carbon-nitrogen bond and 1315-1008 cm^{-1} carbohydrate and lignin carbonyl bond stretching vibration suggests that polar oxygen and nitrogen functional groups had raise onto the surface after the LPPT [47,49], improving the wettability of cork surface through the creation of adhesive bonds with other materials. [35]

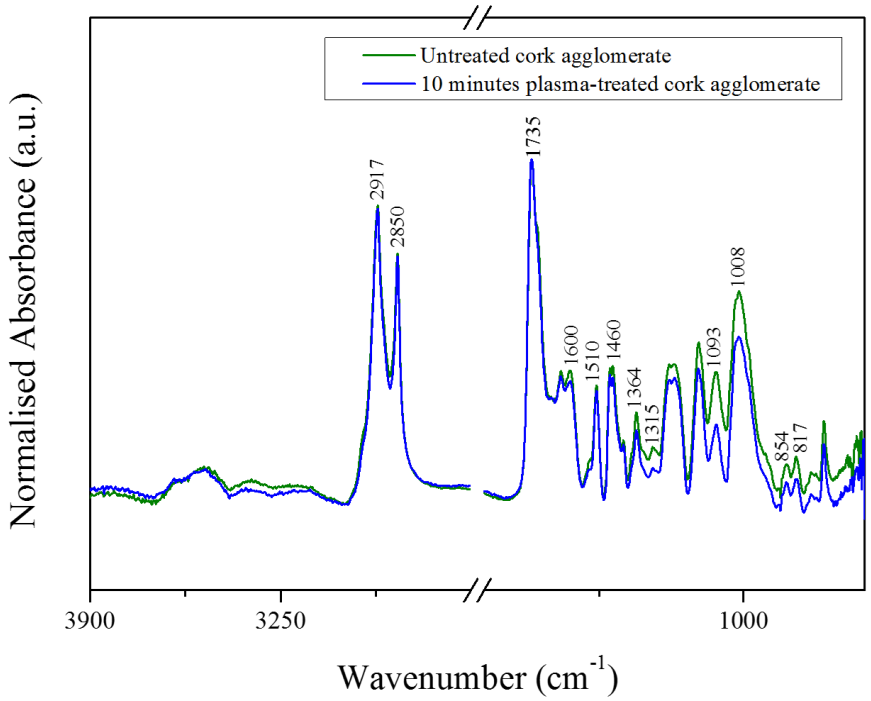

Figure 5 – FTIR spectrum of untreated and 10 minutes plasma treated cork agglomerate samples.

As it is well known, the surface of the untreated cork is hydrophobic, an undeniable characteristic of the material mainly due to the presence of suberin, creating a poor adhesion between untreated cork surface and other materials. [35] Therefore, a high contact angle between deionized water and untreated cork surface is expected. [16] A series of contact angle measurements were performed concerning the changes provoked by the LPPT.

Figure 6 shows the average static contact angle values between deionized water, glycerol, ethylene glycol, and diethylene glycol and the surface of cork agglomerate samples. Results on the samples that experienced LPPT show a major decrease in the static contact angle between the deionized water droplets and the cork agglomerate surface, verifying the switch from a hydrophobic to a hydrophilic behavior. Untreated cork agglomerate has an initial contact angle of 124.4 ± 1.9 º with deionized water (Figure 6A) but as the time of plasma treatment increases the average value of the static contact angle decreases, with the lowest value of 43.3 ± 2.4 º achieved with 10 minutes of plasma treatment (Figure 6B). Nevertheless, at the first minute of LPPT is where the major decrease in the static contact angle, drastically changing the wettability of the cork agglomerate surface. With the time increase of LPPT, there is still a subsequent decrease in the static contact angle but less so than in the first minute. Thus, there is a connection between the decrease of static contact angle and consequently, higher hydrophilicity and the increase of the LPPT time. Hence, it is demonstrated that the wettability of the cork agglomerate surface is boosted by the time exposed to the LPPT.

It is intended that all steps of the planarization process are optimized for the shortest possible time. It is verified by the results that the decrease of the average contact angle is smaller with the increase of the treatment time, making the results obtained by the LPPT very similar after a certain time. Therefore, the plasma treatment was not performed for more than 10 minutes.

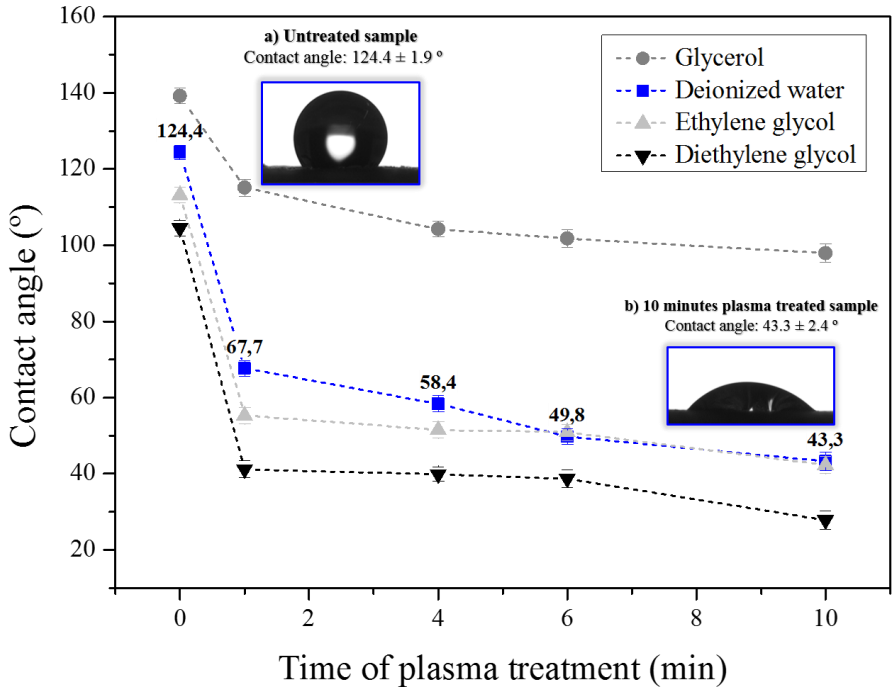

Figure 6 – Average static contact angle of cork agglomerate samples before and after LPPT with deionized water, glycerol, ethylene glycol and diethylene glycol for different treatment times.

The contact angle of a substrate depends on surface factors including surface energy, roughness, and cleanliness of the surface [38], thus results can be explained due to interaction between active species of the O_2 plasma and the cork agglomerate surface, where the hydrophobic

layer is partially decomposed by the LPPT due to the etching process and the creation of polar groups at the surface. [47,51]

Concerning the total surface energy of the cork agglomerate samples, the Wu method using deionized water, glycerol, ethylene glycol, and diethylene glycol average static contact angle values were applied to determine the dispersive and non-dispersive components. Figure 7 displays the obtained results. Also, the work of adhesion for deionized water of each cork agglomerate sample was calculated and the results were displayed in Figure C.1 – Annex C.

Untreated cork displays low surface energy of 8.85 mJ m^{-2}, with a dispersive component 3.1 times higher than the non-dispersive. When LPPT is applied, total surface energy and work of adhesion considerably increase, with the time of plasma treatment influencing this rise. When analyzing the maximum time of LPPT, it is possible to see that surface energy enhances by a factor of 4.8 with a higher increase at the non-dispersive component, reaching 30.45 $mJ.m^{-2}$. Furthermore, the work of adhesion also increased by a factor of 3.4 between the untreated and the 10 minutes plasma-treated sample.

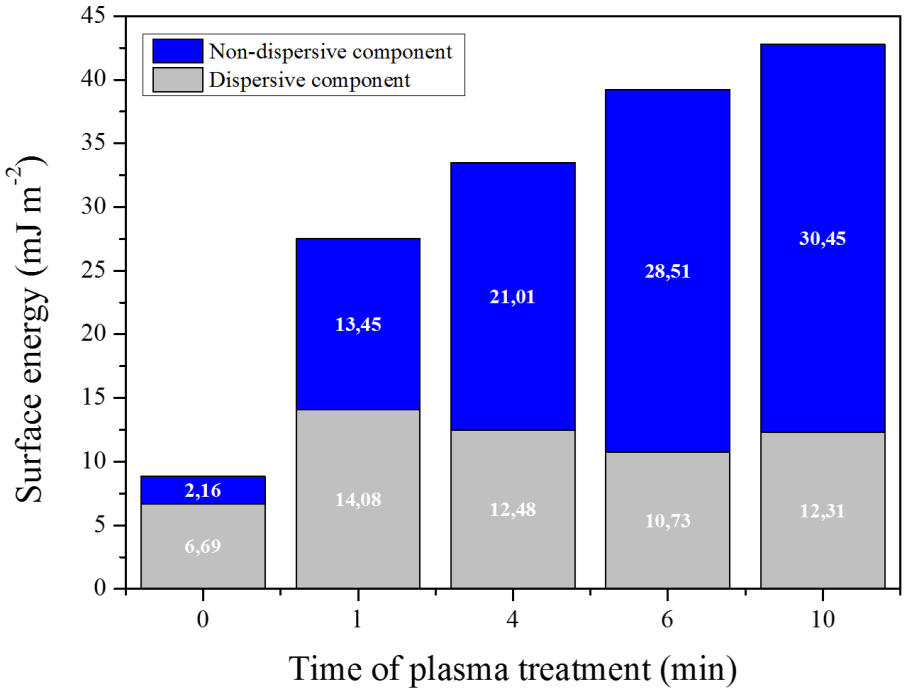

Figure 7 – Surface energy components before and after LPPT on cork agglomerate samples.

For the CNF planarization process, samples of cork agglomerate with 10 minutes of LPPT time were coated with single and double layers using the previously created solutions of CNF. In samples with a double coating layer, the second layer was only applied after air drying at room temperature after the first one (approximately 30 minutes). After all CNF layers were applied in each sample, they were placed in a custom-made frame to prevent curling and dried at room temperature. The coating speed and the temperature were maintained the same through the production of all the samples, with values of 3 m/min and room temperature, respectively. The parameters of production can be consulted in Table B.2 – Annex B. Also, one CNF coated sample without previous LPPT was produced to observe the influence of the plasma treatment in the

creation of the planarization layer. This sample was created using the parameters of sample 80-0.95CNF-1L but without the plasma treatment.

Figure 8 shows FTIR spectra from CNF coated cork agglomerate samples with and without previous 10 minutes plasma treatment, emphasizing the LPPT key role in the way that the planarization layer of CNF is properly coated to the surface of the samples. Through the analysis of the FTIR spectra, it is possible to observe the appearance of characteristic CNF peaks (Figure B.2 – Annex B) such as the hydroxyl group stretching band at 3600-3000 cm^{-1}, methyl and methylene groups C-H stretching vibration at 2914 cm^{-1}, the peak near 1058 cm^{-1} related to hydrophilic carboxylate groups and the typical C-O-C ring vibration related to cellulose at 1031 cm^{-1} in the cork agglomerate sample after the coating step. [54] At the cork agglomerate sample that experienced 10 minutes LPPT, higher absorbance peaks were registered, suggesting the presence of more CNF onto the substrate.

Therefore, the superficial changes caused by the LPPT are essential for the successful application of the CNF planarization layer on the samples, since the hydroxyl groups on the CNF surface [44] will combine with the abundance of carbohydrate and carbonyl polar groups created by the LPPT on the cork agglomerate surface, culminating in stronger hydrogen bonds between the CNF coating layer and the surface of the substrate.

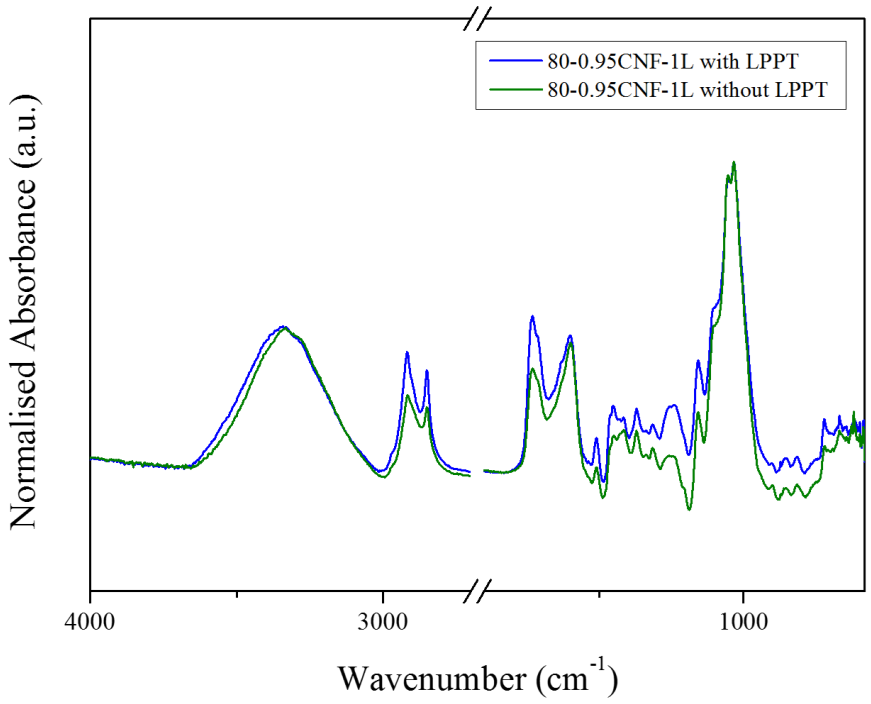

Figure 8 – FTIR spectrum of CNF auto bar coated without LPPT and 10 minutes plasma treated CNF auto bar coated cork agglomerate samples.

Through SEM images from Figures C.2 and C.3 – Annex C, it is possible to observe the successful creation of various CNF planarized samples and analyze the influence that the CNF coating thickness has on the creation of a better quality planarization layer.

Samples coated with the close wound meter bar of 40 μm wet film deposit show significant differences with the change in the CNF weight ratio used to planarize them. Starting with the samples that were coated with the lowest CNF weight ratio (0.60%), a poor planarization layer was achieved. In these samples, it is possible to observe that the honeycomb structure was not uniformly covered (Figure C.2A). Even applying a second layer of CNF (Figure C.2B), the obtained results are still not satisfactory. Similarly, samples coated with the intermediate weight ratio of CNF (0.75%) continue to show a poor overall coating, despite slight improvements especially when the second layer of CNF was applied (Figure C.2C and C.4D). The two coated samples with the highest CNF weight ratio (0.95%) present a surface that is different from the previous samples since a higher CNF weight ratio increases the surface smoothness. [56] Therefore, Figure C.2E and C.4F reveal an effective planarization of the surface of the cork agglomerate, despite the existence of certain areas in which the honeycomb structure is still notorious as pointed out.

The results obtained in the samples coated with the close wound meter bar of 80 μm wet film deposit, shown in Figure C.3 – Annex C, are comparable with those previously mentioned. The use of a higher CNF weight ratio mixture and the application of two layers of CNF on the cork agglomerate create a more uniform surface, and therefore, a better planarization layer, as shown in Figure C.3E and C.5F. At these samples, the honeycomb structure, superficial fractures, and inclusions of the cork agglomerate are almost covered by the CNF, leading to a drastic reduction of the superficial imperfections and, as consequence, to a marked decrease in its roughness. However, the differences caused by the variation in the CNF weight ratio in these samples are not so significant due to the greater deposit of wet film on the substrate surface. This particularity demonstrates that the increase in the thickness of the CNF layer deposited on the substrate possibly has more influence on the creation of a good planarizing layer than the CNF weight ratio used.

Figure 9 shows the average deionized water contact angle values of the CNF auto bar coated samples. The results expose the hydrophilicity of these coated substrates, contrasting with the original hydrophobicity of untreated cork agglomerate (Figure 6).

Surface roughness is a parameter with a great impact on the wettability of the substrate, as smoother substrates tend to have substantially lower contact angles than rougher substrates. [57] As such, we can conclude through the values presented in Figure 9 together with the SEM images of Figure C.2 and C.5 – Annex C, that although the difference between the contact angle values of the samples with one or two layers is not relatively large, there is nevertheless a smoother surface in the samples with the planarizing layer composed of two layers of CNF.

Also, a higher weight ratio of CNF generates a slightly lower average contact angle, indicating a smoother surface [57]. Hence, these results corroborate what was previously mentioned: samples produced with higher CNF weight ratio and the close wound meter bar of 80 μm wet film deposit are way smoother than the others because of the thicker planarization layer.

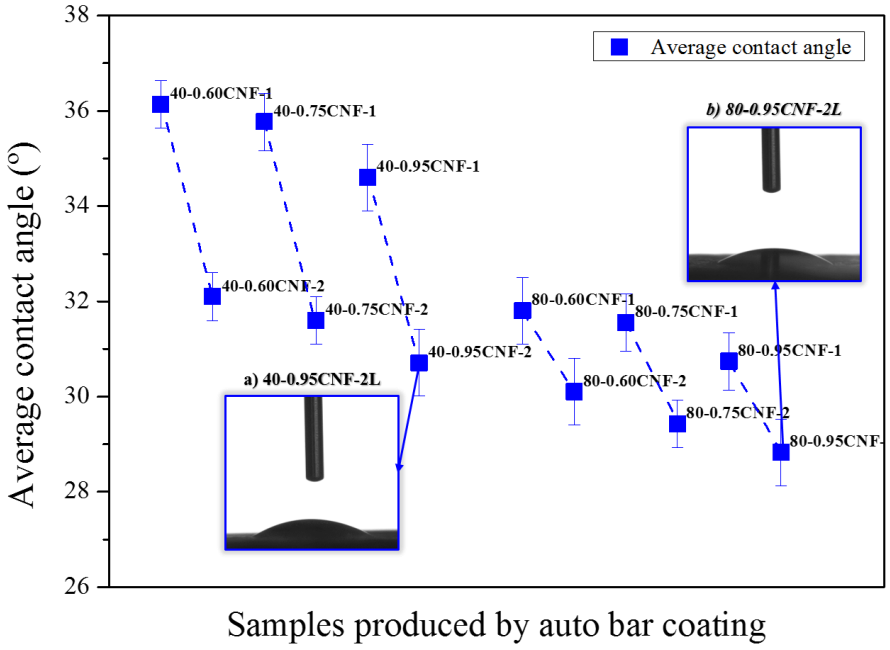

Figure 9 – Average static contact angle of the produced CNF auto bar coated cork agglomerate samples with deionized water. The insets show the samples with lower average static contact angle from each close wound meter bar used at this work.

SEM cross-sectional images of the better-planarized samples from each close wound meter bar used are displayed in Figure 10. Using ImageJ software, five measurements along each sample were done to estimate the average thickness. Firstly, it is possible to observe how CNF covers the surface of the cork agglomerate. After the auto bar coating step, the CNF dries on the surface creating a thin layer that is conformal to the uneven surface and covers the existing irregularities. The results are shown in Table C.1 – Annex C. A higher thickness of the planarization layer can explain the more effective coating displayed by 80-0.95CNF-2L in Figure C.3F – Annex C.

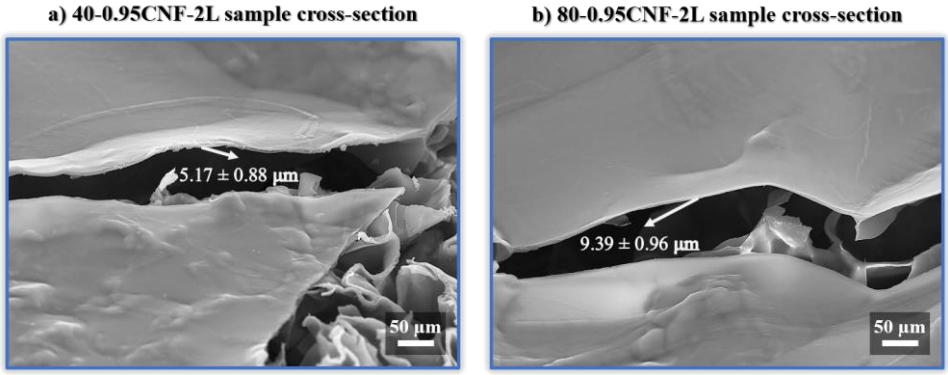

Figure 10 – Cross-section SEM images of a) 40-0.95CNF-2L and b) 80-0.95CNF-2L cork agglomerate samples.

To produce the CNF membrane coated sample, 5 g of bulk CNF were dispersed on 12.5 g of deionized water and stirred using a magnetic stirrer for 15 minutes. Then, the dispersed solution was drop-casted onto a polystyrene Petri dish and left to dry at a controlled temperature of 20ºC and 31% RH. This procedure resulted in the creation of a thin, transparent, and smooth membrane. [44] A 10 minute plasma-treated cork agglomerate sample was then coated following

the same coating parameters of the sample 80-0.95CNF-1L. This CNF layer served also as an adhesive between the previously produced membrane and the cork agglomerate substrate. Without letting the previously coated CNF layer dry, the CNF membrane was laminated onto the sample and placed on a custom-made frame to dry at 22 ºC and 48% RH. The laminated samples with the CNF membrane had their surface fully covered and without any type of cork characteristic superficial defects, as shown by the SEM image in Figure 11. Furthermore, it is also impossible to visualize any cell of the cork honeycomb structure, indicating a drastic reduction in surface roughness since the CNF membrane reduces the porosity of the surface, thus increasing its smoothness. [44] Consequently, the coating performed using a CNF membrane lamination method presents, in comparison to untreated and CNF auto bar coated samples, less superficial roughness and therefore, a more uniform surface. To determine the thickness of the CNF membrane, five measurements using a digital micrometer on the cork agglomerate sample before and after the coating were performed. The results showed that the CNF membrane has a thickness of approximately 20 μm.

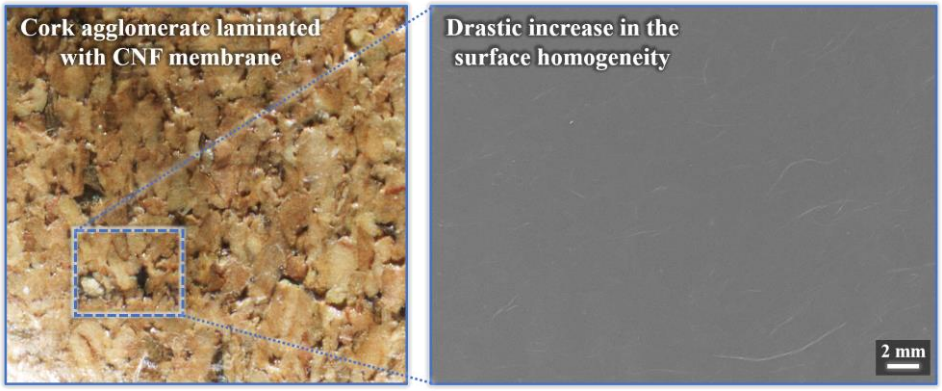

Figure 11 – SEM image (at right) of the CNF membrane coated sample produced.

5.2. UV sensors production and characterization

Substrates coated with 0.95wt. % CNF were used in the production of UV sensors, as this weight ratio of CNF displayed better results. To understand the influence of the planarization layer in the device performance, both untreated and plasma-treated substrates were used in the production of UV sensors for performance comparison. Manual screen-printing was the selected printing technique to produce the UV sensors, as it allows fast production of devices and is a simple technique. [23] 40wt. % ZnO dissolved in aqueous 3wt. % CMC solution with the weight ratio of 40:60 was used as the semiconductor ink to print the first layer of the UV sensor. CMC was used as a binder material due to its viscosity, thickening capability, and good dispersing and stabilizing agent for functional nanostructures. Aqueous 3wt. % CMC was also referred to as the ideal binder concentration to use in screen-printing by Barras et al. [55] This semiconductor layer was printed using a mesh model 77T and dried at room temperature for approximately 5 minutes. After the total drying of the semiconductor layer, conducting carbon ink was used to print the interdigital electrodes layer on top of the semiconductor, using this time a mesh model 120T to improve the printing resolution of this layer. The device was cured at 100ºC in a hotplate for 10 minutes. A schematic representation of the final printed UV sensor is shown in Figure 12, with a ZnO photosensitive layer of 6.5 x 6.5 mm and a carbon electrode layer with three pairs of 0.5 mm

interdigital fingers gapped also by 0.5 mm between them. This procedure was applied on seven types of substrates as Table C.2 – Annex C displays, for subsequent performance comparison between them.

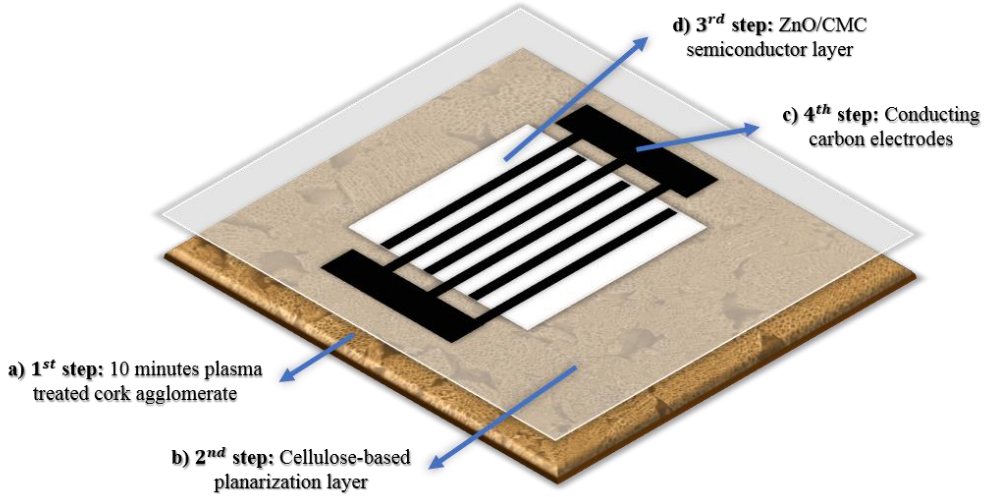

Figure 12 – Schematic representation of the UV sensor produced on the cellulose-based planarized substrate

Figure 13 highlights the effect of the planarized CNF layer at the macroscopic level. The untreated cork agglomerate sample (shown in Figure 13A) has visible surface defects and irregularities. The samples with the planarization layer (shown in Figure 13 from B to E) showed a clear improvement in the uniformity of the semiconductor layer of ZnO, with fewer holes, cracks, and irregularities. Hence, increasing the thickness of the planarized layer results in a noticeable decrease in areas with defects for the ZnO layer which might be an indication of a possible increase in electrical performance. The conductive carbon layer also has fewer irregularities, which is crucial to avoid the occurrence of discontinuities, holes, and cracks. As for aesthetics, the characteristic untreated cork agglomerate pattern and color is conserved despite using the planarization layer, which can be important for future applications concerning the device's appearance design.

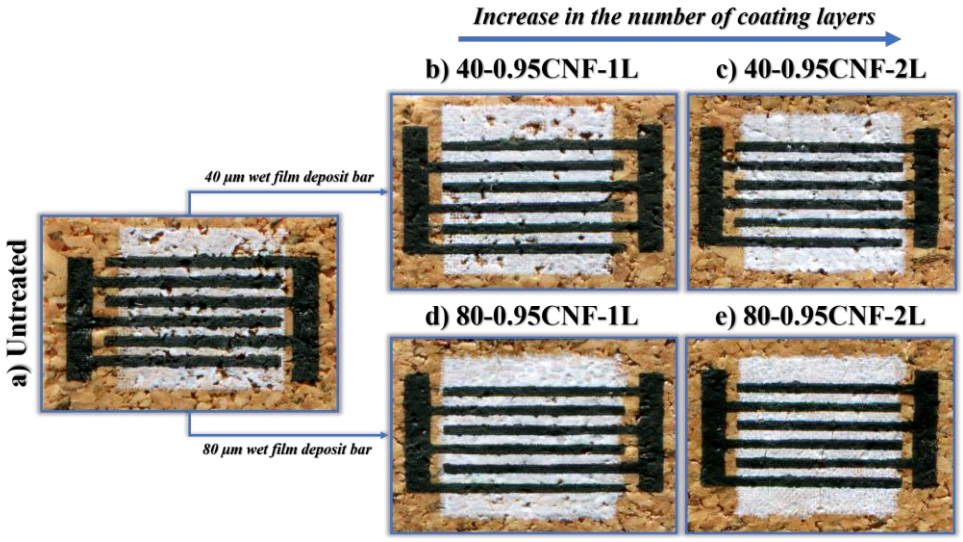

Figure 13 – Decrease of the UV sensor superficial defects in the cork agglomerate substrate with the increase of the CNF planarization layer thickness.

For electrical characterization of the produced UV sensors, 1 V of bias voltage was continuously applied between the interdigital electrodes of the sensors, and four completed ON/OFF cycles were performed on each substrate type, with a 60 s time step. Three light conditions were performed inside a dark chamber: dark (UV light OFF) and light (UV light ON) with two different intensities. To guarantee good reliability of the results, five produced UV sensors from each selected substrate were electrically characterized, at a known RH (shown at the photoresponse curve figures). The photoresponse curves of the UV sensors screen-printed on cork agglomerate substrates without planarization are represented in Figure C.4 – Annex C. Sensors printed on the untreated and 10 minutes plasma-treated substrate showed low replicability between them because both types of substrates have a non-uniform surface. The non-uniformity of the not planarized cork agglomerate substrate leads to a device performance randomness: if the UV sensor is printed in a substrate area with fewer surface defects, the performance will be better and vice versa.

It is desirable to achieve high electrical performance on UV sensors so that they perform the intended task properly. [58] As such, high performance is translated by high on/off current ratio, fast response, and recovery times, and large photoresponse current. [28] The better performance achieved in areas with fewer surface defects is explained by the ZnO UV-sensing mechanism. The working principle is based on the O_2 vacancies that exist on the surface of the ZnO nanoparticles. Exposure to UV light with photon energy above the ZnO bandgap photogenerates electron-hole pairs, with the holes reducing the depletion zone through the discharge of absorbed negative ions which follows desorption by the surface, creating free electrons.

Consequently, the measured photocurrent will increase. Hence with the absence of UV light, electrical conductivity suffers a reduction caused by the capturing of free electrons by the absorption of molecules with high O_2 concentration at the vacancy site, depleting the particle's surface. Absorption and desorption process can be described by the next three Equations [17]:

$$O_2(g) + e^- \rightarrow O_2^-(ad) \quad (1)$$

$$hv \rightarrow e^- + h^+ \quad (2)$$

$$h^+ + O_2^-(ad) \rightarrow O_2(g) \quad (3)$$

Photoresponse current (I_{ph}) is defined by Equation (4):

$$I_{ph} = I_{light} - I_{dark} \quad (4)$$

Where I_{dark} is the dark current and I_{light} is the photocurrent under UV illumination. [28]

Figure C.4 – Annex C also shows that higher I_{ph} was achieved with higher intensity of the UV light, reaching a value of approximately 21.39 µA for the best performing untreated sample when applying 8.66 W cm^{-2} at the last ON/OFF light cycle with 51% RH. For the 10 minutes plasma-treated samples, the results show a lower maximum I_{ph} value achieved then at untreated samples, with approximately 16.21 µA for the best performing plasma-treated sample with the same characterization conditions of the untreated substrate. Although these samples experienced

LPPT, they were not planarized, and therefore, the performance depends on whether the area where they were printed has better or worse surface characteristics.

No noteworthy photocurrent degradation along the four completed ON/OFF light cycles was observed in both types of substrates, ensuring stability and consistent performance.

Dark current (I_{dark}) values were low for both types of substrates along the four completed ON/OFF light cycles, with values under 12 and 47 nA for the untreated and 10 minutes plasma-treated substrate samples, respectively. This indicates that most of the electrons in the ZnO layer are depleted by the surface-adsorbed oxygen molecules. [28]

The sensor's photosensitivity (p_s) is defined by Equation (5):

$$p_s = \frac{I_{ph}}{I_{dark}} \tag{5}$$

With a higher p_s ratio suggesting a better quality of the produced sensor. [28] Untreated and 10 minutes plasma-treated substrates present a p_s of 1.78×10^3 and 3.45×10^2 for the 8.66 W cm^{-2} light condition, respectively.

The ideal UV sensors translate their performance into a quadratic photoresponsive curve due to fast rise and fall times. Rise time (t_{rise}) is defined as the time taken by the UV sensor to reach 90 % of the I_{ph} from 10 %. In contrast, fall time (t_{fall}) is the time taken to reach 10% of I_{ph} from 90 % [17], with t_{rise} and t_{fall} values decreasing with the increase of light intensity. [59]

Figure 14 shows average t_{rise} and t_{fall} values for the UV sensor that reached the highest I_{ph} value on untreated and 10 minutes plasma-treated substrate along the four completed light ON/OFF cycles. t_{rise} values were lower when the light intensity was higher for both substrates, with the untreated substrate having the most pronounced difference. Further, t_{fall} value at both types of substrates also suffered a decrease with increasing light intensity but only with a small variation on the 10 minutes plasma-treated substrate.

Nevertheless, the UV sensors produced with the untreated and plasma-treated substrates present photoresponse curves that do not fully approach a quadratic shape due to relatively long t_{rise} and t_{fall} values. The decreasing rate of adsorbed O_2 ions relates to the t_{rise} of the UV sensor. With the UV light hitting on the UV sensor, the surface band-bending will cause the generated holes to migrate towards the surface to neutralize the O_2 ions existing there, leading to the desorption of O_2 molecules. The height of the band-bending will decrease due to the continuity of this process, slowing down the holes migration speed and making the UV sensor have long t_{rise}. When the UV light stops reaching the UV sensor, the O_2 molecules will gradually adsorb on the ZnO surface, creating O_2 ions. This adsorption process is divided into two parts: the physical process and the chemical process. First occurs the physical process through a concentration gradient. As the physical process happens, a decrease of the O_2 density gradient near the ZnO surface takes place, slowing down the O_2 adsorption and generating longer t_{fall}. Therefore, the velocity of adsorbing O_2 molecules that create O_2 ions determine the t_{fall} of the UV sensor. [58]

Since t_{rise} and t_{fall} values are influenced by the adsorption and desorption rates of O_2 molecules from the ZnO surface, it is possible to conclude that on the untreated sample the UV-induced O_2 desorption rate is much smaller than the O_2 adsorption rate on the ZnO surface and

for the 10 minutes plasma-treated sample the rates are quite similar. The interdigital electrode spacing can also not be ideal, with shorter spacing contributing to shorter t_{rise} and t_{fall} values. [58-60] Another possibility is a "shadow effect" caused by the printing of the interdigital electrodes on top of the ZnO semiconductor layer. This reduces the ZnO layer area that is exposed to UV light. Also, the UV lamp can change from the UV light ON to the UV light OFF state slowly, influencing the t_{rise} and t_{fall} measurements of the UV sensor.

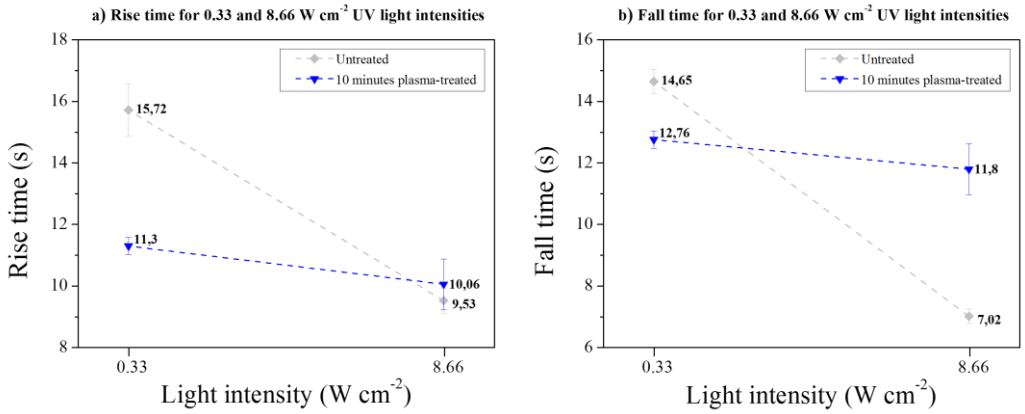

Figure 14 – Average t_{rise} and t_{fall} values for sensors printed on untreated and 10 minutes plasma treated substrate samples for both UV light intensities used along the four completed ON/OFF light cycles. The dashed lines are given just as guide and have no physical meaning.

Contrarily, planarized substrate samples have a more homogenous surface. The sensors printed on the 40-0.95CNF-2L and 80-0.95CNF-2L substrates display notable improvements in replicability, with more accurate printing results as Figures C.5 and C.6 – Annex C display. This improvement is more noticeable in substrates that have two layers of CNF. Although the application of only one layer of CNF presents a reasonable coverage of the cork agglomerate surface, there are still some surface imperfections and some areas with noticeable honeycomb cellular structure not planarized, as seen previously in Figures C.2 and C.3 – Annex C. When the second layer of CNF is applied, those faulty covered zones will reduce, creating a general improvement of surface homogeneity. Again, no noteworthy photocurrent degradation along the four completed ON/OFF light cycles was observed in all types of auto bar coated substrates, ensuring stability and consistent performance.

Figures C.5 and C.6 – Annex C show that higher I_{ph} on the planarized substrates was also achieved at the higher intensity of the UV light, with 80-0.95CNF-1L and 80-0.95CNF-2L attaining the highest I_{ph} values from all tested substrates. I_{ph} reaches approximately 92.04 and 133.38 µA in the 8.66 W cm^{-2} light intensity condition at the last ON/OFF cycle with 54% RH for 80-0.95CNF-1L and 80-0.95CNF-2L substrates, respectively. Best performing UV sensors of 40-0.95CNF-1L and 40-0.95CNF-2L substrates disclose lower I_{ph} values than the other two coated substrates (39.24 and 75.37 µA, respectively) but still higher than the untreated sample for the same characterization conditions. Accordingly, performing the auto bar coating with the close wound meter bar of 80 µm wet film deposit creates higher I_{ph} results. Higher I_{ph} was achieved by the 80-0.95CNF-1L and 80-0.95CNF-2L substrates since they have the smoothest surface between all produced auto bar coated samples, as Figures C.5E and C.5F – Annex C show, with

fewer cracks and discontinuities in the printed layers. [44] As the ZnO UV-sensing mechanism is based on surface reactions, lower surface imperfections improve the achieved I_{ph}. [17]

Figure 15 shows the relation between the UV light intensity and the induced photocurrent of the 80-0.95CNF-2L substrate. It is possible to see the increase in photocurrent as UV light intensity also increases.

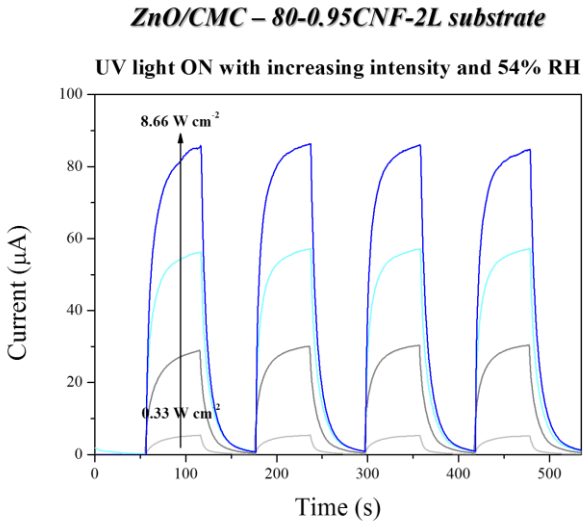

Figure 15 – Influence of different UV light intensities on the induced photocurrent at the 80-0.95CNF-2L substrate.

I_{dark} values were higher for all types of auto bar coated substrates when compared to the untreated substrate samples, along the four completed ON/OFF light cycles, with the highest I_{dark} value registered at the 80-0.95CNF-2L substrate sample but still under 120 nA. I_{dark} is mostly influenced by the barrier weight generated from electron depletion between the ZnO grain boundaries, having lower values when more electrons are depleted. Therefore, at the planarized samples the electrons are not being totally depleted by the surface adsorbed O_2 molecules, translating into an increase of I_{dark}. Further, p_s was calculated for all planarized substrate samples.

The p_s was higher for the 80-0.95CNF-1L and 80-0.95CNF-2L substrates, with values of 4.61×10^2 and 1.1×10^3 for the 8.66 W cm^{-2} light condition, respectively. For the 40-0.95CNF-1L and 40-0.95CNF-2L substrates, p_s values were of 2.68×10^2 and 3.84×10^2 for the 8.66 W cm^{-2} light condition, respectively. The lower p_s results for all planarized substrates except 80-0.95CNF-2L are induced by the higher I_{dark} measured mentioned before. To solve this problem, the ZnO layer thickness should be close to the depleted layer caused by the O_2 adsorption. With this characteristic, the UV sensor will have major improvements on the I_{dark}.[58] Likewise, reducing the electrode spacing can be a possible solution [59] still achievable by manual screen-printing technique. [24]

Figures 16 and 17 show average t_{rise} and t_{fall} values for the UV sensor that reached the highest I_{ph} value on each auto bar coated substrate type along the four completed light ON/OFF cycles. Like the untreated substrate samples, t_{rise} and t_{fall} values were again lower when the light intensity was higher. Further, there is an increase for both t_{rise} and t_{fall} values when compared to the untreated cork agglomerate substrate samples, also not featuring the ideal quadratic photoresponsive curve. This is justified by slower O_2 molecule adsorption and desorption rates if

compared with the untreated substrate samples. [58] UV-induced O_2 desorption rates and the O_2 adsorption rates on the ZnO surface were alike especially at 80-0.95CNF-1L and 80-0.95CNF-2L samples due to similar t_{rise} and t_{fall} values. However, at the 40-0.95CNF-1L sample, the t_{rise} and t_{fall} values are not similar, with lower t_{fall} than t_{rise} as previously registered at the untreated sample. [59]

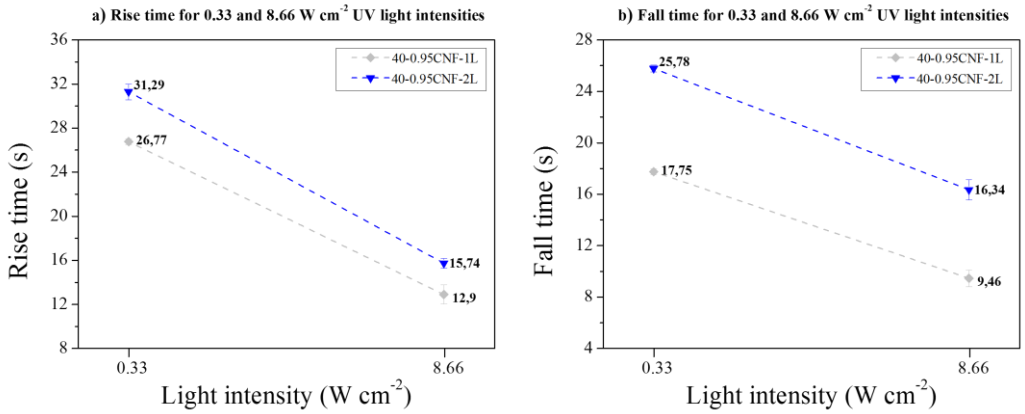

Figure 16 – Average t_{rise} and t_{fall} values for sensors printed on 40-0.95CNF-1L and 40-0.95CNF-2L substrate samples for both UV light intensities used along the four completed ON/OFF light cycles. The dashed lines are given just as guide and have no physical meaning.

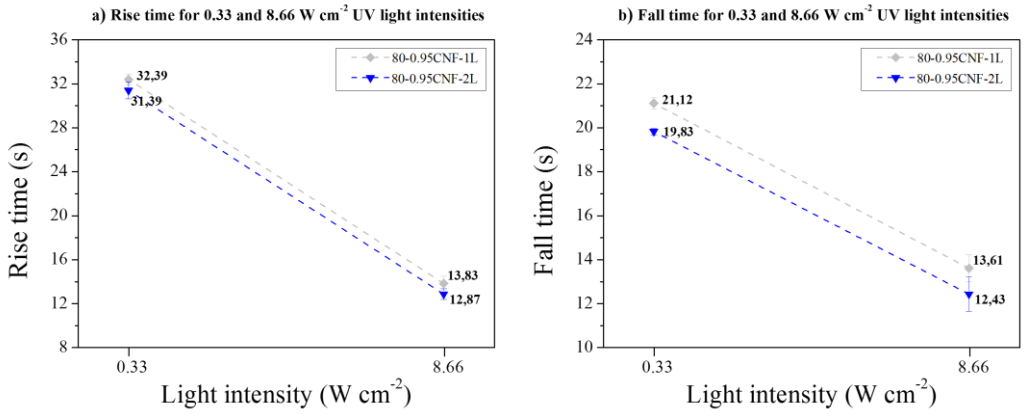

Figure 17 – Average t_{rise} and t_{fall} values for sensors printed on 80-0.95CNF-1L and 80-0.95CNF-2L substrate samples for both UV light intensities used along the four completed ON/OFF light cycles. The dashed lines are given just as guide and have no physical meaning.

A UV sensor was screen-printed using the same production parameters on a glass substrate. The glass substrate was used as a reference since it is rigid and non-porous and therefore, allows the creation of much smoother, homogeneous, and continuous layers at the UV sensor, allowing better performance. [17] The glass substrate was subjected to UV light pre-treatment for 30 minutes to clean and activate the surface, previously to printing. Figure 18 shows the photoresponse curves of UV sensors produced on glass and 80-0.95CNF-2L substrates. It is possible to observe that the UV sensor assembled in the planarized cork agglomerate substrate presented a higher I_{ph} than the one in the glass substrate. The observed I_{ph} decreasing tendency throughout the four UV light ON cycles may be explained by the carrier scattering caused by residual charges in the trap level. As the I_{dark} increases along the four UV light ON cycles, the trapped carriers are not totally released and the decrease of the I_{ph} occurs. [60]

I_{dark} is significatively higher for the 80-0.95CNF-2L substrate sample, with the planarized substrate sample displaying I_{dark} under 120 nA as opposed to the under 18 nA of the glass substrate sample. The lower I_{dark} of the glass substrate guarantees higher p_s for the UV sensor assembled on this substrate. Therefore, higher p_s is achieved at the glass substrate. The UV sensor assembled on the glass substrate displays a photoresponse curve close to the ideal quadratic photoresponsive curve and consequently, t_{rise} and t_{fall} are lower than the planarized cork agglomerate substrate. Nevertheless, it should be noted that the surface of the cork agglomerate is different from glass in terms of roughness and homogeneity. As such, the impressive results obtained by the 80-0.95CNF-2L substrate demonstrate the surface transformation that is caused by the CNF planarization layer. Furthermore, through the UV sensor improvements mentioned before, the planarized cork agglomerate substrate can still achieve equal or better results at I_{dark} values and t_{rise} and t_{fall}.

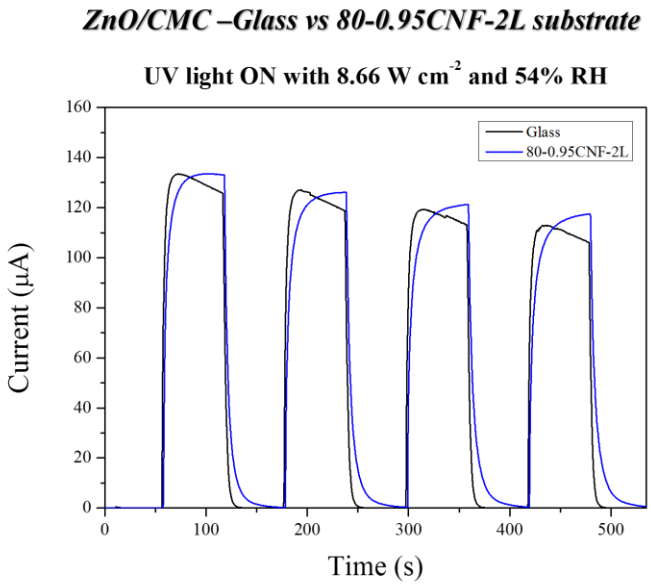

Figure 18 – Comparison of the photoresponse curves of UV sensors assembled on 80-0.95CNF-2L and glass substrates.

Figure 19 displays the photoresponse curves of planarized substrates by lamination of the CNF membrane on the cork agglomerate surface. Unlike auto bar coated substrates, the UV sensors assembled on planarized substrates through the lamination of a CNF membrane showed less replicability in electrical performance between the produced sensors despite the smoothest substrate surface. These results can be explained by the shrinkage that occurs in the drying of the samples. As the adhesive CNF layer has deionized water in its composition, during the drying of the laminated membrane with the substrate it evaporates, and the coated substrate shrinks. [61] Although the drying of the samples is done in a custom-made frame that prevents shrinkage and curling, it ends up occurring slightly. Posteriorly, when handled in the screen-printing process, the shrunk substrate is damaged with the generation of cracks on the surface of the membrane, as Figure C.7 – Annex C shows. To overcome the shrinking and curling of the samples, the drying method must be optimized. Laboratory work suggested that the creation of a custom-made frame with the exact dimensions of the produced samples to place for the drying step can generate better results and prevent the sample borders from curling.

Lower I_{ph} was achieved by the 0.95CNF-M substrate at the 8.66 W cm^{-2} UV light intensity when compared with the auto bar coated substrates. However, at 0.33 W cm^{-2}, a higher I_{ph} was registered with a value of 12.03 µA at the last ON/OFF cycle with 53% RH. I_{dark} values are alike to those of the 80-0.95CNF-2L sample with the UV light intensity of 8.66 W cm^{-2}. However, when the lower UV light intensity of 0.33 W cm^{-2} is applied to the sensor, the I_{dark} value stays under 39 nA. Therefore, I_{dark} is 1.90 times lower than the one registered at the 80-0.95CNF-2L sample. Due to the lower I_{dark} measured, p_s at the lower UV light intensity is superior in this type of substrate. The 0.95CNF-M substrate presents a p_s of 30.79, greater than 10.69 of the 80-0.95CNF-2L substrate, and 10.33 of untreated cork agglomerate substrate. These results suggest that with a lamination method that prevents the curling of the substrate better results can be achieved.

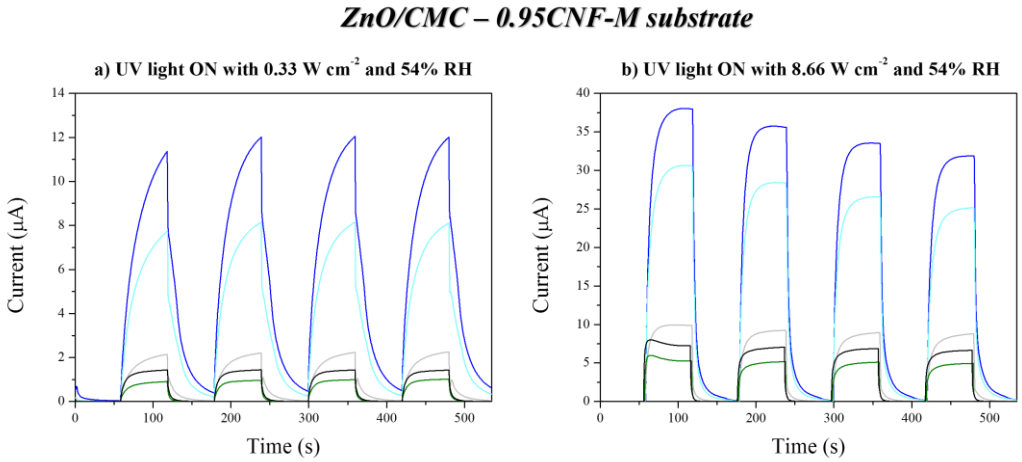

Figure 19 – Photoresponse curves of five screen-printed ZnO UV sensors on CNF membrane laminated substrate samples along four ON/OFF cycles for two UV light intensities.

Average t_{rise} and t_{fall} values for the 0.95CNF-M substrate UV sensor that has the best performance are shown in Figure 20. t_{rise} and t_{fall} values were lower when the applied UV light intensity to the sensor was higher, like the UV sensors assembled onto auto bar coated substrates. Overall, the results obtained at this type of substrate are alike the ones of the auto bar coated substrates, with an increase for both t_{rise} and t_{fall} values when compared to the untreated cork agglomerate substrate samples also justified by slower O_2 molecules adsorption and desorption rates than the untreated substrate samples as previously mentioned. [58]

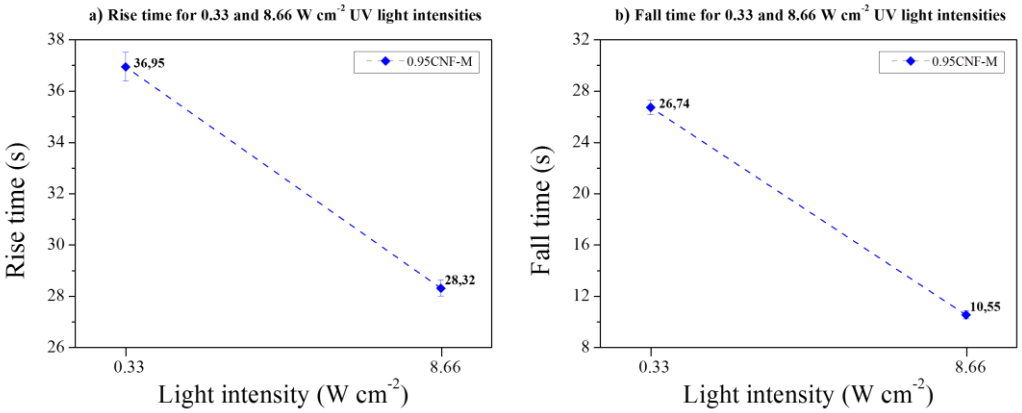

Figure 20 – Average t_{rise} and t_{fall} values for sensors printed on CNF membrane laminated substrate samples for both UV light intensities used along the four completed ON/OFF light cycles. The dashed lines are given just as guide and have no physical meaning.

A bending test was performed on all planarized cork agglomerate samples so the flexibility outside their original planar shape could be analyzed. This test was done to evaluate the possibility of UV sensors assembled on the planarized substrates being used, for example, in wearable devices. These devices create great challenges for their production, as it is necessary to combine high performance with favorable mechanical properties such as flexibility. [62]

The planarized samples were subjected to a 15 mm radius cylinder and left in that bent position for 24 hours at a temperature of 21ºC and 51% RH to simulate a real working scenario. After 24 hours, the UV sensors were removed from the cylinder and measured in their planar form. The mechanical stress caused by bending deformation led to the loss of functionality in all sensors except for the one assembled on the 40-0.95CNF-1L substrate.

Figure 21 shows the large loss of performance of the UV sensor assembled onto the 40-0.95CNF-1L substrate, with I_{ph} suffering a decrease from 75.37 µA to 96.89 pA at the 8.66 W cm^{-2} UV light intensity condition. Also, the stability and consistency of the UV sensor were compromised.

As previously mentioned, the ZnO UV-sensing mechanism is largely affected by surface defects. [17] Consequently, the noticed decrease in the performance and stability of the UV sensors is driven by the breakdown of conductive electrode lines and the formation of cracks in the ZnO semiconductor layer, as Figure C.8 – Annex C shows.

Notwithstanding, this test was performed with the smallest radius cylinder available, causing high strain. A more comprehensive bending test using multiple cylinders with a larger radius will unveil the possibility of the UV sensors assembled on the auto bar coated substrates work in a non-planar form.

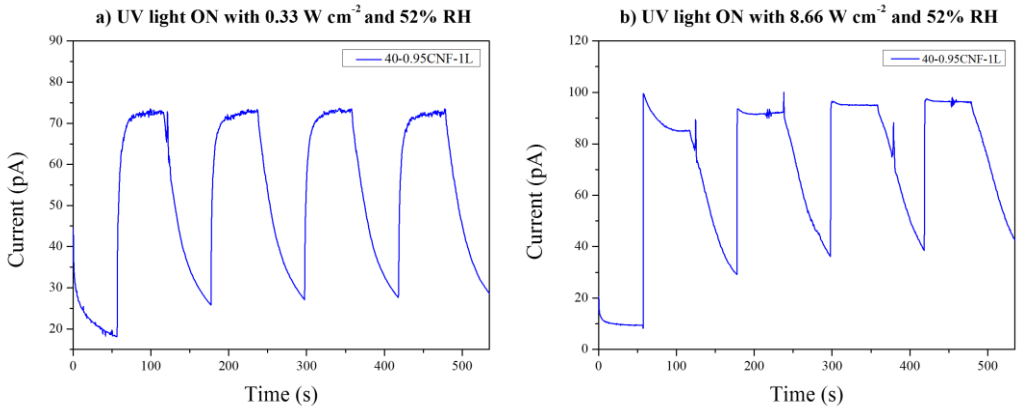

Figure 21 – Photoresponse curve after 24 hours bending test in a 15 cm radius cylinder of an UV sensor printed 40-0.95CNF-1L substrate for both UV light intensities used along the four completed ON/OFF light cycles.

6. CONCLUSIONS

In this work, it is possible to state that the surface characteristics of cork have been improved using low energy methods for its use as a substrate in printed electronic devices. Moreover, produced planarized substrates were successfully used as a substrate for fully screen-printed UV sensors, proving that cork can be used as a sustainable and low-cost substrate for printed electronics.

Within the planarization process, the LPPT plays a fundamental role due to the change in surface wettability, allowing better adhesion of the CNF to cork without changing its chemical properties. For the auto bar coated samples, the use of a higher concentration of CNF together with the application of two layers of CNF creates planarized samples with a smoother surface mainly due to the thicker CNF planarization layer created. CNF membrane laminated samples also show excellent roughness improvements through the total coverage of cork surface imperfections but take more process time compared to the auto bar coating method.

Overall, the planarized substrate creates an improvement in the UV sensor's production and electrical performance results. One of the main advantages of using the planarized substrate is the increase in replicability and accuracy in printing results, which may be essential when producing these devices on a large scale. Also, higher I_{ph} was achieved even with the substrate sample with the thinnest planarization layer. However, higher I_{dark} and longer t_{rise} and t_{fall} registered by the planarized samples are still problems to be studied and solved in future work. Contrarily, printing the UV sensors on substrates that only experienced LPPT does not show any upgrades in replicability or performance. The comparison with a glass substrate shows that the best performing planarized substrate reaches higher I_{ph} than a rigid and non-porous substrate, but with longer t_{rise} and t_{fall}. The substrates planarized through CNF membrane lamination show better performance at the lowest UV light intensity tested, with the results suggesting that with an improved lamination and drying method this substrate can achieve overall better performance.

The bending test reveals the need for a deeper study to fully understand the flexibility of the planarized substrates, as now the performed bending test caused the breakdown of the conducting electrode lines in the UV sensor and the formation of cracks in the ZnO semiconductor layer. Nevertheless, it should be noted that this bending test was performed with the smallest radius cylinder available at the laboratory, causing much more strain to the sample as compared to higher radius cylinders. Therefore, performing bending tests with higher radius cylinders is essential to fully analyze the flexibility of the produced planarized substrate.

Also, it should be taken into consideration that the obtained results and their replicability in all untreated or planarized substrates were also influenced by the slight variations of the user's technique throughout the screen-printing process of the sensors. Therefore, some discrepancies between produced samples may be caused by the operator. To overcome this problem, an automatic screen-printing station can be used, as the printing is no longer done manually.

7. FUTURE PERSPECTIVES

Although cork is one of the oldest materials known to man and being utterly studied, the application of cork in electronics is still a topic with limited research carried out so far, only with few publications available. Therefore, there is space for future improvement and better optimization of all the steps carried out in this work. Still, the successful creation of a planarized cork agglomerate substrate accomplished at this work opens the door to the use of cork as a substrate for a wide range of printed electronic devices.

UV-irradiation could also be an efficient method to activate the cork surface since the improvement of adhesion proprieties on various types of hydrophobic polymers have been reported. [63] Also, this method can be applied at atmospheric pressure and ambient temperature, which facilitates its large-scale application. Therefore, with correct optimization, this method can achieve the same or better results than LPPT. [64]

Concerning the planarization layer, several aspects can be improved towards a more effective planarization. First, the water content of the CNF coating formulations must have special attention. Even with the drying of the coated samples at a custom-made frame, the high-water content caused light curling to the coated cork agglomerates. Therefore, drying in an optimized controlled environment and the addition of a natural-based plasticizer can solve this problem. Plus, to improve the overall uniformity of the planarization layer, the addition to the CNF suspension of CMC or another cellulose derivative that possesses the ability to disperse fibers and reduce their flocculation, can be a good solution. [65,66] Moreover, other coating methods can be more efficient than the methods used. Spray coating is an interesting technique for future research as it allows the creation of a very thin and uniformly distributed coating layer also using CNF. [67] Also, surface analysis by three-dimensional profilometry could be an excellent technique to reach a better understanding of the roughness and homogeneity of the CNF planarized samples.

The manual screen-printing technique showed the total capability to be used in the production of UV sensors in a laboratory environment. For the quality of the sensors produced to be excellent, the rheological properties of the inks used in printing were adjusted considering the characteristics of the substrate. As such, to avoid short-circuits and poor print resolution, a better adjustment of the semiconductor ZnO ink, even if slight, can give better results. Besides, the use of an automatic screen-printing station can greatly improve the quality and replicability of the sensors due to the elimination of printing errors associated with the operator's technique. As opposed to manual screen-printing, this automatic station also allows large-scale printing of UV sensors quickly and efficiently. Further, the possibility of defining several printing parameters on the automatic screen-printing station makes it possible to study how changes in these parameters will also affect the performance of the sensors.

Furthermore, bending tests with more types of round mods should be done on all planarized samples. Respectively, round mods of larger curvature radius should be used to fully understand the maximum bending limits of the samples and evaluate the possibility for using these planarized substrates in future wearable applications such as health and environmental monitoring. [62]

BIBLIOGRAPHY

[1] Irimia-Vladu, Mihai. (2014). "Green" electronics: biodegradable and biocompatible materials and devices for sustainable future (vol 43, pg 588, 2014). Chemical Society Reviews. 43. 6470-6470.

[2] Lovley, Derek. (2017). e-Biologics: Fabrication of Sustainable Electronics with "Green" Biological Materials. mBio. 8. 10.1128/mBio.00695-17

[3] King, Alexander. (2016). When agendas align: Critical materials and green electronics. 1-6. 10.1109/EGG.2016.7829825.

[4] Chang, Joseph & Facchetti, Antonio & Reuss, Robert. (2017). A Circuits and Systems Perspective of Organic/Printed Electronics: Review, Challenges, and Contemporary and Emerging Design Approaches. IEEE Journal on Emerging and Selected Topics in Circuits and Systems. PP. 1-20. 10.1109/JETCAS.2017.2673863.

[5] Zardetto, Valerio & Brown, Thomas & Reale, Andrea & Di Carlo, Aldo. (2011). Substrates for Flexible Electronics: A Practical Investigation on the Electrical, Film Flexibility, Optical, Temperature, and Solvent Resistance Properties. Journal of Polymer Science Part B: Polymer Physics. 49. 638 - 648. 10.1002/polb.22227.

[6] Chang, Joseph & Ge, Tong & Sanchez-Sinencio, E.. (2012). Challenges of printed electronics on flexible substrates. Midwest Symposium on Circuits and Systems. 582-585. 10.1109/MWSCAS.2012.6292087.

[7] Gil, L.; Marques, Isabel P. Cork wastes as energy sources. In: WASTES'2013 – 2nd International Conference Wastes: solutions, treatments and opportunities, Book of Proceedings, Braga, Portugal, 11-13 September, 2013, p. 123-126

[8] Gil, Luis. (2009). Cork Composites: A Review. Materials. 2. 10.3390/ma2030776.

[9] Gil, L. Cortiça. In: M. Clara Gonçalves, Fernanda Margarido (eds.), "Ciência e Engenharia de Materiais de Construção", IST, 2012, cap. 13, p. 663-715, ISBN 978- 989-8481-17-7

[10] Cork Quality Council "Cork Quality Council – Industry Statistics." [Online]. Available: https://www.corkqc.com/pages/industry-statistics/. [Accessed: 10-Jan-2020]

[11] Associação Portuguesa da Cortiça, "APCOR – Social e Económica."[Online]. Available: http://www.apcor.pt/montado/sustentabilidade/sustentabilidade-social-e-economica/. [Accessed:10-Jan2020]

[12] Gil, Luis. (2014). Cork: a strategic material. Frontiers in Chemistry. 2. 0.3389/fchem.2014.00016.

[13] Silva, Susana & Sabino, Marcos & Fernandes, Emanuel & Correlo, Vitor & Boesel, Luciano & Reis, Rui L.. (2005). Cork: Properties, capabilities and applications. International Materials Reviews. 50. 345-365. 10.1179/174328005x41168.

[14] Pereira, Helena. (1988). Chemical composition and variability of cork from Quercus suber L. Wood Science and Technology. 22. 211-218. 10.1007/BF00386015.

[15] Gil, Luis. (2015). New Cork-Based Materials and Applications. Materials. 8. 625-637. 10.3390/ma8020625

[16] Knapic, Sofia & Oliveira, Vanda & Machado, José & Pereira, Helena. (2016). Cork as a building material: a review. European Journal of Wood and Wood Products. 74. 10.1007/s00107-016-1076-4.

[17] Figueira, Joana & Gaspar, Cristina & Carvalho, José Tiago & Loureiro, Joana & Fortunato, Elvira & Martins, R. & Pereira, Luis. (2019). Sustainable Fully Printed UV Sensors on Cork Using Zinc Oxide/Ethylcellulose Inks. Micromachines. 10. 601. 10.3390/mi10090601.

[18] Tan, Mein & Owh, Cally & Chee, Pei Lin & Kyaw, Aung & Kai, Dan & Loh, Xian Jun. (2016). Bio-degradable Electronics: Cornerstone for sustainable electronics and transient applications. J. Mater. Chem. C. 4. 10.1039/C6TC00678G.

[19] Khan, Saleem & Dahiya, Ravinder & Lorenzelli, Leandro. (2014). Technologies for Printing Sensors and Electronics Over Large Flexible Substrates: A Review. IEEE Sensors Journal. PP. 10.1109/JSEN.2014.2375203.

[20] Goncalves, Ricardo & Rima, Sergi & Magueta, Roberto & Pinho, Pedro & Collado, Ana & Georgiadis, Apostolos & Hester, Jimmy & Carvalho, Nuno & Tentzeris, Manos. (2015). RFID-Based Wireless Passive Sensors Utilizing Cork Materials. IEEE Sensors Journal. 15. 1-1. 10.1109/JSEN.2015.2472980.

[21] Leenen, Mark & Arning, Volker & Thiem, Heiko & Steiger, Juergen & Anselmann, Ralf. (2009). Printable Electronics: Flexibility for the Future. 10.1002/9783527627387.ch2.

[22] P. J. Wojcik, Printable Organic and Inorganic Materials for Flexible Electrochemical Devices, Universidade Nova de Lisboa, Faculdade de Ciências e Tecnologia, 2013.

[23] S. J. Rubin, Development of eco-friendly ZnO inks for paper-based printed electronics, Universidade Nova de Lisboa, Faculdade de Ciências e Tecnologia, 2017.

[24] Subramanian, Vivek & Chang, Josephine & Vornbrock, Alejandro & Huang, Daniel & Jagannathan, Lakshmi & Liao, Frank & Mattis, Brian & Molesa, Steven & Redinger, David & Soltman, Daniel & Volkman, Steven & Zhang, Qintao. (2008). Printed Electronics For Low-Cost Electronic Systems: Technology Status and Application Development. ESSDERC 2008 - Proceedings of the 38th European Solid-State Device Research Conference. 17 - 24. 10.1109/ESSCIRC.2008.4681785.

[25] Amin, Dr. Gul. (2020). ZnO and CuO Nanostructures: Low Temperature Growth, Characterization, their Optoelectronic and Sensing Applications.

[26] Hassinen, Tomi & Alastalo, Ari & Eiroma, Kim & Tenhunen, Tiia-Maria & Kunnari, Vesa & Kaljunen, Timo & Forsström, Ulla & Tammelin, Tekla. (2015). All-Printed Transistors on Nano Cellulose Substrate. MRS Advances. -1. 1-6. 10.1557/adv.2015.31.

[27] Sang, Liwen & Liao, Meiyong & Sumiya, Masatomo. (2013). A Comprehensive Review of Semiconductor Ultraviolet Photodetectors: From Thin Film to One-Dimensional Nanostructures. Sensors (Basel, Switzerland). 13. 10482-518. 10.3390/s130810482.

[28] Bai, Suo & Wu, Weiwei & Qin, Yong & Cui, Nuanyang & Bayerl, Dylan. (2011). High-Performance Integrated ZnO Nanowire UV Sensors on Rigid and Flexible Substrates. Advanced Functional Materials. 21. 4464 - 4469. 10.1002/adfm.201101319.

[29] Wang, Zhong. (2009). Nanostructures of Zinc Oxide. Materials Today. 7. 26-33. 10.1016/S1369-7021(04)00286-X.

[30] Pimentel, Ana & Samouco, Ana & Nunes, Daniela & Araújo, Andreia & Martins, Rodrigo & Fortunato, Elvira. (2017). Ultra-Fast Microwave Synthesis of ZnO Nanorods on Cellulose Substrates for UV Sensor Applications. Materials. 10. 1308. 10.3390/ma10111308.

[31] Razeghi, Manijeh & Rogalski, Antoni. (1996). Semiconductor Ultraviolet Detectors. Journal of Applied Physics. 79. 7433 - 7473. 10.1063/1.362677.

[32] Gaspar, Cristina & Olkkonen, Juuso & Passoja, Soile & Smolander, Maria. (2017). Paper as Active Layer in Inkjet-Printed Capacitive Humidity Sensors. Sensors (Switzerland). 17. 10.3390/s17071464.

[33] Shin, Hyeonwoo & Roh, Jeongkyun & Song, Jiyoung & Roh, Heebum & Kang, Chan-Mo & Lee, Taesoo & Park, Gunbaek & An, Kunsik & Kim, Jun Young & Kim, Hyoseok & Kwak, Jeonghun & Lee, Changhee & Kim, Hyeok. (2019). Highly Stable Organic Transistors on Paper Enabled by a Simple and Universal Surface Planarization Method. Advanced Materials Interfaces. 6. 1801731. 10.1002/admi.201801731.

[34] Oliveira, Vanda & Van den Bulcke, Jan & Van Acker, Joris & De Schryver, Thomas & Pereira, Helena. (2016). Cork structural discontinuities studied with X-ray microtomography. Holzforschung. 70. 87-94. 10.1515/hf-2014-0245.

[35] Abenojar, Juana & Barbosa, Ana & Del Real, Juan & Silva, L.F.M. & Martínez Casanova, Miguel. (2013). Effect of surface treatments on natural cork: Surface energy, adhesion, and acoustic insulation. Wood Science and Technology. 10.1007/s00226-013-0599-7.

[36] Tendero, Claire & Dublanche-Tixier, C. & Tristant, P. & Desmaison, Jean & Leprince, Philippe. (2006). Atmospheric Pressure Plasmas: A Review. Spectrochimica Acta Part B-atomic Spectroscopy - SPECTROCHIM ACTA PT B-AT SPEC. 61. 2-30. 10.1016/j.sab.2005.10.003.

[37] Calvimontes, Alfredo & Mauersberger, Peter & Nitschke, Mirko & Dutschk, Victoria & Simon, Frank. (2011). Effects of oxygen plasma on cellulose surface. Cellulose. 18. 803-809. 10.1007/s10570-011-9511-5.

[38] Oliveira, Fernando & Erkens, Laura & Fangueiro, Raul & Souto, António. (2012). Surface Modification of Banana Fibers by DBD Plasma Treatment. Plasma Chemistry and Plasma Processing. 32. 10.1007/s11090-012-9354-3.

[39] Sanchis, M.R. & Blanes, Vicente & Blanes, M. & Garcia-Sanoguera, David & Balart, R.. (2006). Surface modification of low density polyethylene (LDPE) film by low pressure O2 plasma treatment. European Polymer Journal. 42. 1558-1568. 10.1016/j.eurpolymj.2006.02.001.

[40] Petasch, W & Kegel, B & Schmid, H & Lendenmann, K & Keller, H.. (1997). Low-pressure plasma cleaning: A process for precision cleaning applications. Surface & Coatings Technology - SURF COAT TECH. 97. 176-181. 10.1016/S0257-8972(97)00143-6.

[41] Wu, An-Ju & Hsu, Shih-Hua & Chen, Wei-Han & Liu, Kuan-Hsien & Tsai, Chia-Hung & Tu, Chun-Hao & Liu, Chu-Yu & Chiang, Ming-Feng & Lin, Yu-Chieh. (2018). P-129: Planarization Effect on Electrical Performances of Organic Thin Film Transistors. SID Symposium Digest of Technical Papers. 49. 1584-1586. 10.1002/sdtp.12313.

[42] Kumar, Vinay & Elfving, Axel & Koivula, Hanna & Bousfield, Douglas & Toivakka, Martti. (2016). Roll-to-Roll Processed Cellulose Nanofiber Coatings. Industrial & Engineering Chemistry Research. 55. 10.1021/acs.iecr.6b00417.

[43] Bardet, Raphael & Bras, Julien. (2014). Cellulose Nanofibers and Their Use in Paper Industry. 10.1142/9789814566469_0013.
[44] Hoeng, Fanny & Denneulin, Aurore & Bras, Julien. (2016). Use of nanocellulose in printed electronics: A review. Nanoscale. 8. 10.1039/C6NR03054H.
[45] Hamada, Hitomi & Bousfield, Douglas. (2010). Nanofibrillated cellulose as a coating agent to improve print quality of synthetic fiber sheets. Tappi Journal. 9. 25-29. 10.32964/TJ9.11.25.
[46] Baley, Christophe & Busnel, Frederic & Grohens, Yves & Sire, Olivier. (2006). Influence of chemical treatments on surface properties and adhesion of flax fibre–polyester resin. Composites Part A: Applied Science and Manufacturing. 37. 1626-1637. 10.1016/j.compositesa.2005.10.014.
[47] Oliveira, Fernando & Silva, Etienne & Carmo, Sidney & Steffens, Fernanda & Souto, António. (2014). Functionalization of Natural Cork Composite with Microcapsules after Plasma Treatment. Advances in Materials Science and Engineering. 2014. 10.1155/2014/685829.
[48] Oliveira, Fernando & Fernandes, Marta & Carneiro, Noemia & Souto, António. (2013). Functionalization of wool fabric with phase-change materials microcapsules after plasma surface modification. Journal of Applied Polymer Science. 128. 10.1002/app.38325.
[49] Lopes, Marta & Neto, C. & Barros, Antonio & Rutledge, Douglas & Delgadillo, Ivonne & Gil, Ana. (2000). Quantitation of aliphatic suberin in Quercus suber L. Cork by FTIR spectroscopy and solid-state 13C-NMR spectroscopy. Biopolymers. 57. 344-51. 10.1002/1097-0282(2000)57:6<344::AID-BIP40>3.0.CO;2-#.
[50] Shimizu, Renato & Demarquette, N.. (2000). Evaluation of surface energy of solid polymers using different models. Journal of Applied Polymer Science, 76, 1831-1845. Journal of Applied Polymer Science. 76. 1831 - 1845. 10.1002/(SICI)1097-4628(20000620)76:12<1831::AID-APP14>3.0.CO;2-Q.
[51] Silva, E. A., Fernando Ribeiro Oliveira, S. Carmo, F. Steffens and A. Souto. “Characterization of natural cork agglomerate functionalised by plasma treatment.” (2013).
[52] Sacui, Iulia & Nieuwendaal, Ryan & Burnett, Daniel & Stranick, Stephan & Jorfi, Mehdi & Weder, Christoph & Foster, E. Johan & Olsson, Richard & Gilman, Jeffrey. (2014). Comparison of the Properties of Cellulose Nanocrystals and Cellulose Nanofibrils Isolated from Bacteria, Tunicate, and Wood Processed Using Acid, Enzymatic, Mechanical, and Oxidative Methods. ACS Applied Materials & Interfaces. 6. 6127–6138. 10.1021/am500359f.
[53] Silva, Cristina & Kano, Fabiany & Rosa, D.. (2019). Lignocellulosic Nanofiber from Eucalyptus Waste by a Green Process and Their Influence in Bionanocomposites. Waste and Biomass Valorization. 11. 10.1007/s12649-019-00610-3.
[54] Gaspar, Diana Filipa Pereira, Active cellulose-based substrates for application in eletronic devices, Universidade Nova de Lisboa, Faculdade de Ciências e Tecnologia, 2019.
[55] Barras, Raquel & Cunha, Inês & Gaspar, Diana & Fortunato, Elvira & Martins, R. & Pereira, Luis. (2017). Printable cellulose-based electroconductive composites for sensing elements in paper electronics. Flexible and Printed Electronics. 2. 10.1088/2058-8585/aa5ef9.
[56] Afra, Elyas & Mohammadnejad, Saeed & Saraeyan, Ahmadreza. (2016). Cellulose nanofibils as coating material and its effects on paper properties. Progress in Organic Coatings. 101. 455-460. 10.1016/j.porgcoat.2016.09.018.
[57] Simonsen, Galina & Eriksen, Øyvind & Gregersen, Øyvind. (2012). TEMPO-oxidized cellulose nanofiber films: Effect of surface morphology on water resistance. Cellulose. 19. 10.1007/s10570-012-9721-5.
[58] Xu, Qi & Cheng, Li & Meng, Leixin & Wang, Zhe & Bai, Suo & Tian, Xiaoqiang & Jia, Xiaofeng & Qin, Yong. (2019). Flexible Self-Powered ZnO film UV Sensor with High Response. ACS Applied Materials & Interfaces. 11. 10.1021/acsami.9b09264.
[59] Kim, Sun & Moon, Dong-Il & Seol, Myeong-Lok & Kim, Beomseok & Han, Jin-Woo & Meyyappan, Meyya. (2018). Wearable UV Sensor Based on Carbon Nanotube-Coated Cotton Thread. ACS Applied Materials & Interfaces. 10. 10.1021/acsami.8b16153.
[60] Tang, Shiang-Feng & Hong, Yuehua & Chen, Zhangwei & Lao, Changshi & Lu, Youming & Yang, Zhichao & Zhu, Youhua & Liu, Xinke. (2020). ZnO UV Photodetectors Modified by Ag Nanoparticles Using All-Inkjet-Printing. Nanoscale research letters. 15. 176. 10.1186/s11671-020-03405-x.
[61] Oh, Kyudeok & Rajabi-Abhari, Araz & Wanhee, Im & Lee, Hak Lae. (2019). Stress Development in Cellulose Nanofibril-Containing Pigment Coating Layer during Drying. Industrial & Engineering Chemistry Research. 58. 10.1021/acs.iecr.9b02906.
[62] Cai, Sa & Xu, Xiaojie & Yang, Wei & Chen, Jiaxin & Fang, Xiaosheng. (2019). Materials and Designs for Wearable Photodetectors. Advanced Materials. 31. 10.1002/adma.201808138.

[63] Sham, Man Lung & Li, Jing & Ma, Peng-Cheng & Kim, Jang-Kyo. (2009). Cleaning and Functionalization of Polymer Surfaces and Nanoscale Carbon Fillers by UV/Ozone Treatment: A Review. Journal of Composite Materials - J COMPOS MATER. 43. 1537-1564. 10.1177/0021998308337740.

[64] d'Eon, Jeffrey & Zhang, Wei & Chen, Li & Berry, Richard & Zhao, Boxin. (2017). Coating cellulose nanocrystals on polypropylene and its film adhesion and mechanical properties. Cellulose. 24. 10.1007/s10570-017-1222-0.

[65] Nazari, Behzad & Bousfield, Douglas. (2016). Cellulose nanofibers influence on properties and processing of paperboard coatings. Nordic Pulp and Paper Research Journal. 31. 511-520. 10.3183/NPPRJ-2016-31-03-p511-520.

[66] Mazhari Mousavi, Seyyed Mohammad & Afra, Elyas & Tajvidi, Mehdi & Bousfield, Douglas & Dehghani-Firouzabadi, M.. (2017). Cellulose nanofiber/carboxymethyl cellulose blends as an efficient coating to improve the structure and barrier properties of paperboard. Cellulose. 24. 10.1007/s10570-017-1299-5.

[67] Brodin, Fredrik Wernersson, Øyvind Weiby Gregersen, and Kristin Syverud. " Cellulose nanofibrils: Challenges and possibilities as a paper additive or coating material – A review". Nordic Pulp & Paper Research Journal 29.1 (2014): 156-166. 10.3183/npprj-2014-29-01-p156-166

ANNEXES

1. Annex A

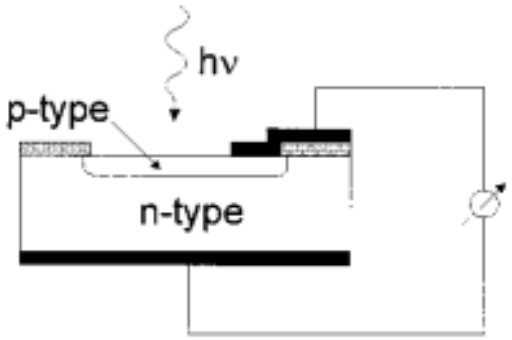

Figure A.1 – Working principle of a semiconductor detector.
Adapted from [30].

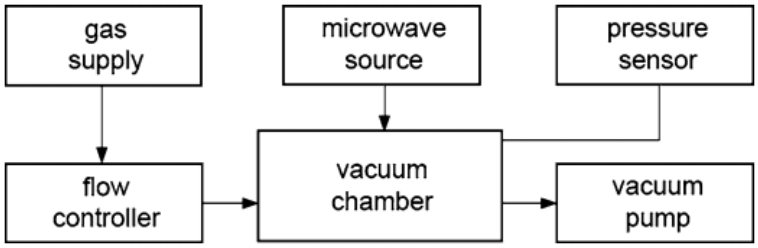

Figure A.2 – Scheme of the plasma instrumentation.
Adapted from [37].

2. Annex B

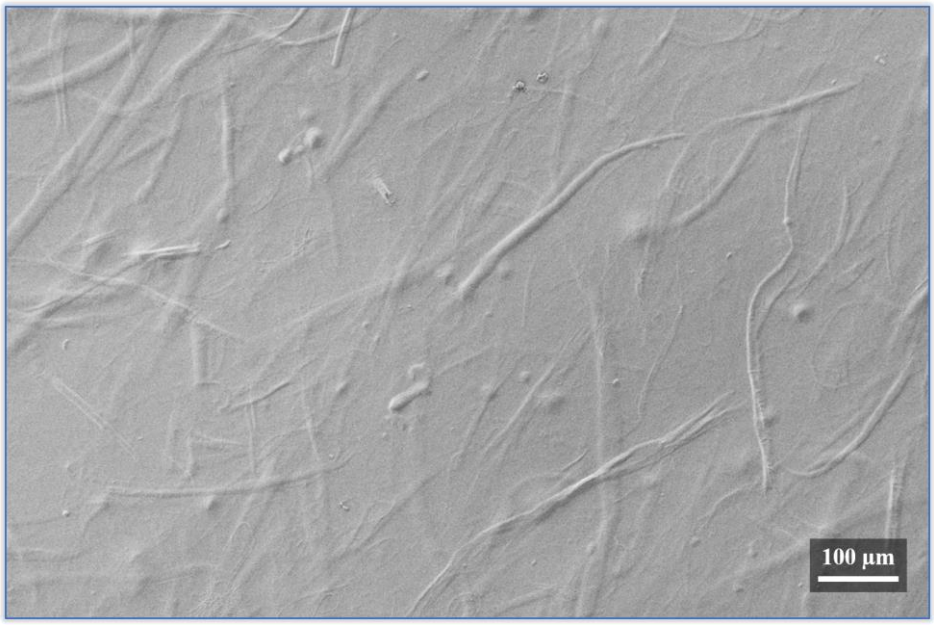

Figure B.1 – SEM image of bulk 0.95wt. % CNF used at this work.

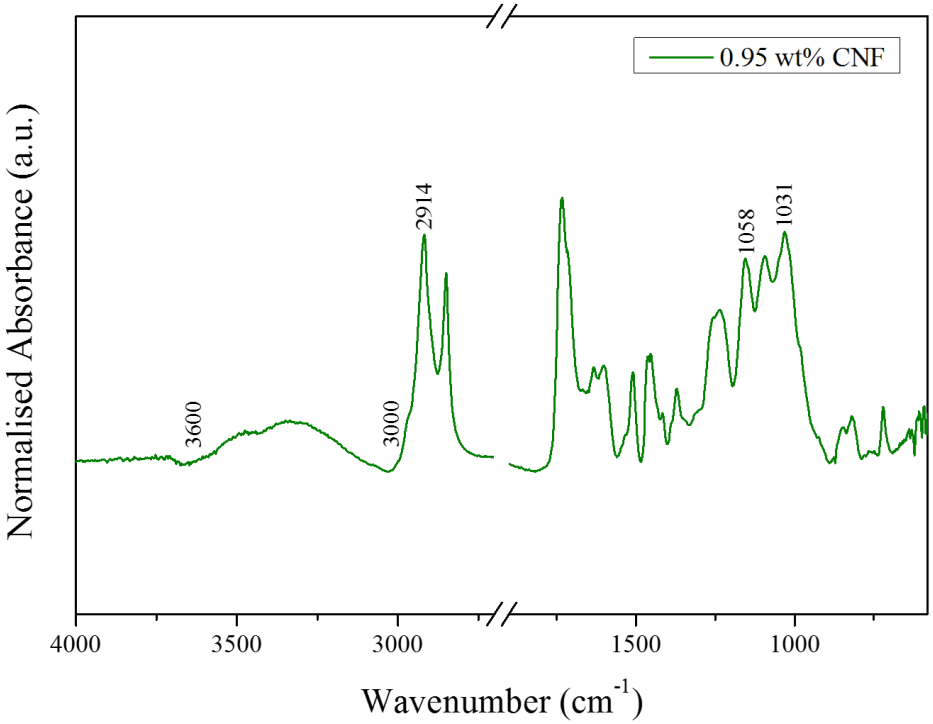

Figure B.2 – FTIR spectrum of bulk 0.95wt. % CNF used at this work.

Table B.1 – Nomenclature and parameters used on the plasma treatment of the cork agglomerate samples.

Sample	p (mBar)	p_w (mBar)	P (W)	T (min)
C1	0.15	0.30	75	1
C4				4
C6				6
C10				10

Table B.2 – Nomenclature and parameters used on the production of LPPT treated CNF auto bar coated cork agglomerate samples.

Sample	Bar wet film deposit (µm)	CNF weight ratio (%)	Number of layers
40-0.95CNF-1L	40	0.95	1
40-0.95CNF-2L			2
40-0.75CNF-1L	40	0.75	1
40-0.75CNF-2L			2
40-0.6CNF-1L	40	0.60	1
40-0.60CNF-2L			2
80-0.95CNF-1L	80	0.95	1
80-0.95CNF-2L			2
80-0.75CNF-1L	80	0.75	1
80-0.75CNF-2L			2
80-0.60CNF-1L	80	0.60	1
80-0.60CNF-2L			2

Table B.3 – Surface energy components of deionized water, glycerol, ethylene glycol, and diethylene glycol.

Liquid	γ_D (mJ m^{-2})	γ_{ND} (mJ m^{-2})	γ (mJ m^{-2})
Deionized Water	22.1	50.7	72.8
Glycerol	37.4	26.0	63.4
Ethylene glycol	30.1	17.6	47.7
Diethylene glycol	31.7	12.7	44.4

3. Annex C

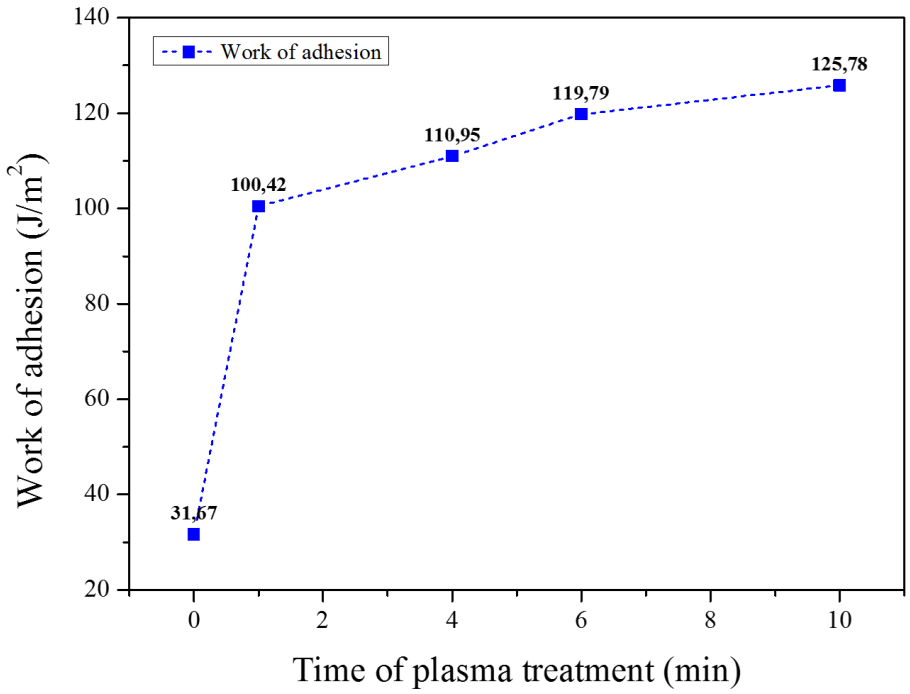

Figure C.1 – Work of adhesion before and after LPPT of deionized water on cork agglomerate samples.

Table C.1 – Thickness of auto bar coated produced CNF planarizing layers.

Sample	Thickness (μm)
40-0.95CNF-2L	5.17 ± 0.88
80-0.95CNF-2L	9.39 ± 0.96

Table C.2 – Types of cork agglomerate substrate used at the UV sensor producing.

Type of substrate	Used close wound meter bar film deposit (µm)	Number of coating layers	Membrane coating
Untreated cork agglomerate	-	-	×
10 minutes plasma treated	-	-	×
10 minutes LPPT plus 0.95CNF coating	80	$\frac{1}{2}$	×
	40	$\frac{1}{2}$	×
10 minutes LPPT plus 0.95CNF membrane coating	80	1	✓

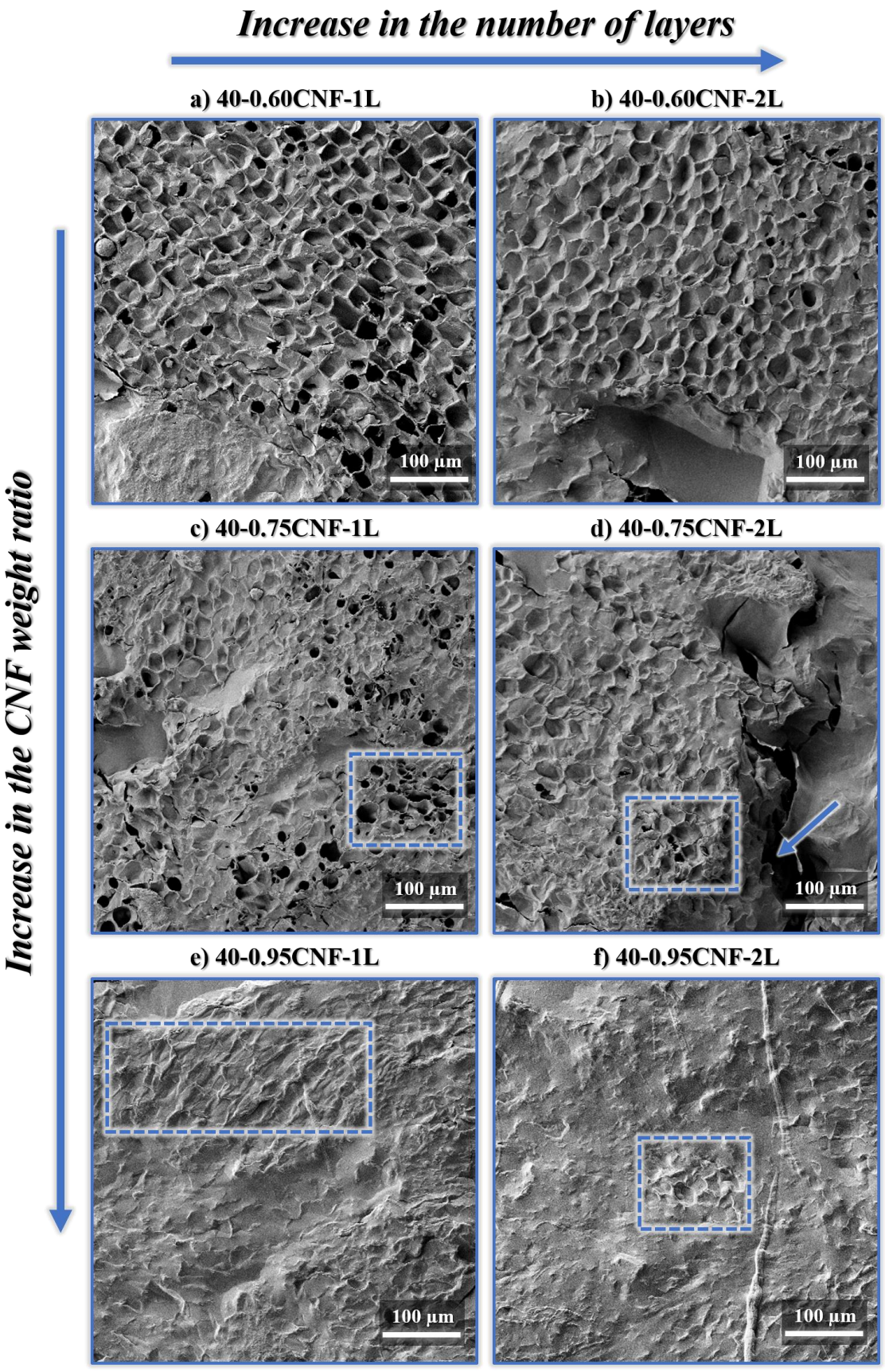

Figure C.2 – SEM images of the different CNF coated samples produced by auto bar coating method with the close wound meter bar of 40 µm wet film deposit.

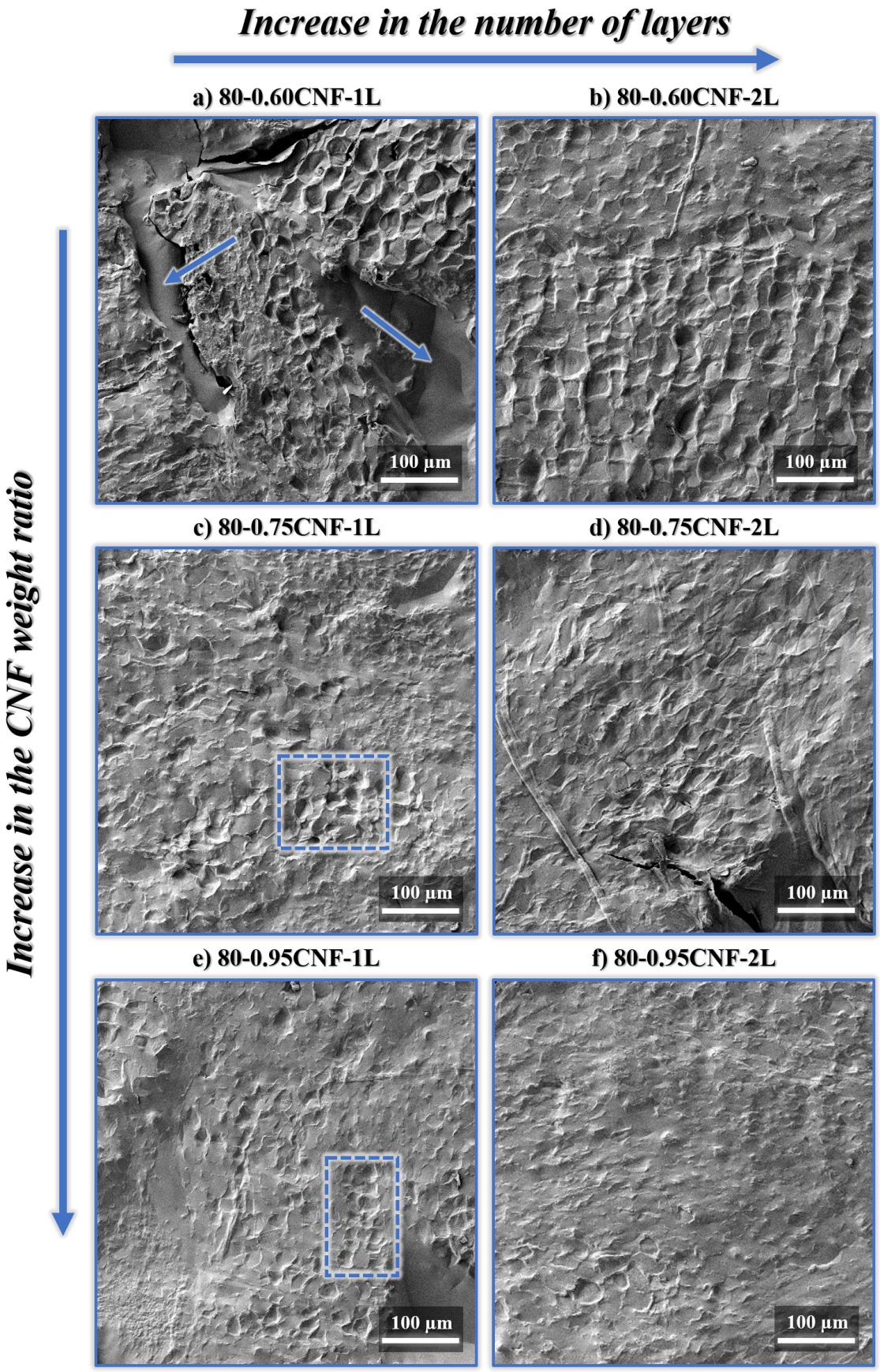

Figure C.3 – SEM images of the different CNF coated samples produced by auto bar coating method with the close wound meter bar of 80 µm wet film deposit.

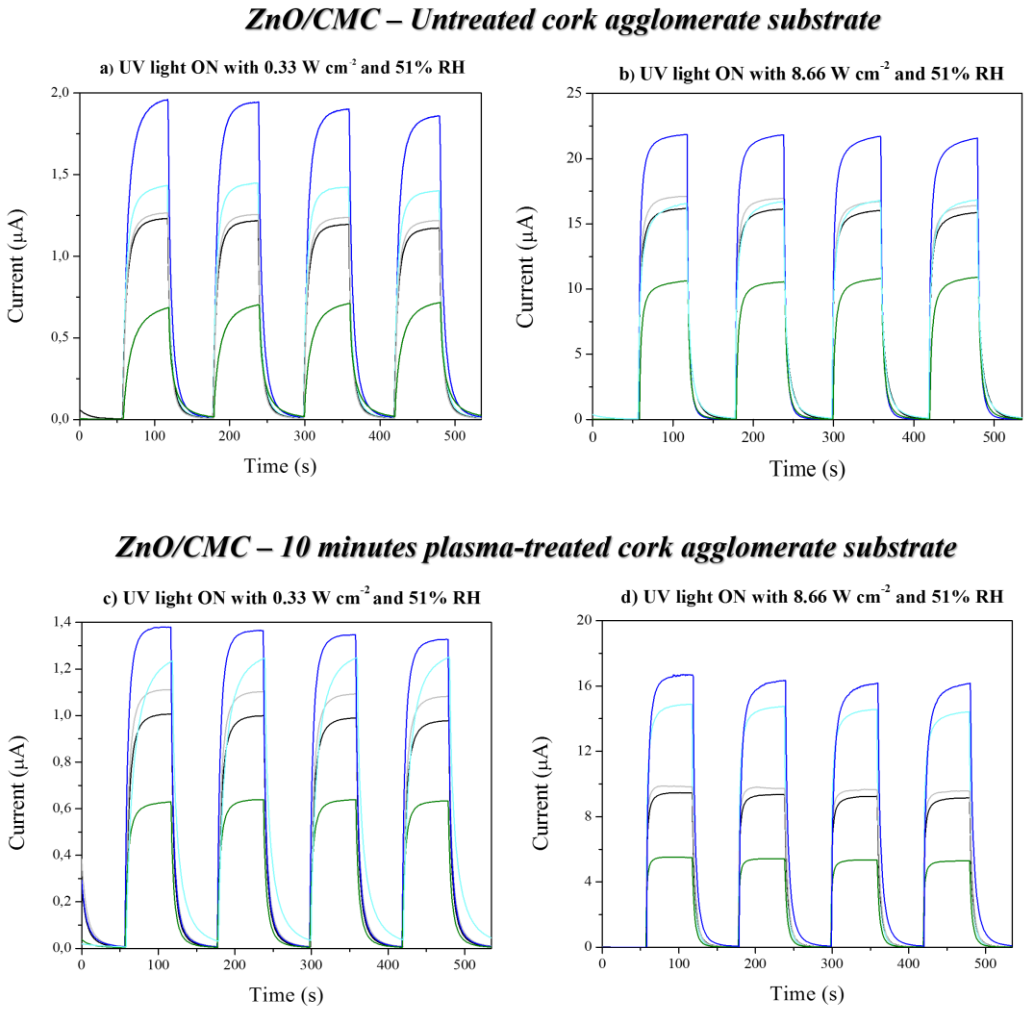

Figure C.4 – Photoresponse curves of five screen-printed ZnO UV sensors on untreated and 10 minutes plasma treated substrate samples along four ON/OFF cycles for two UV light intensities.

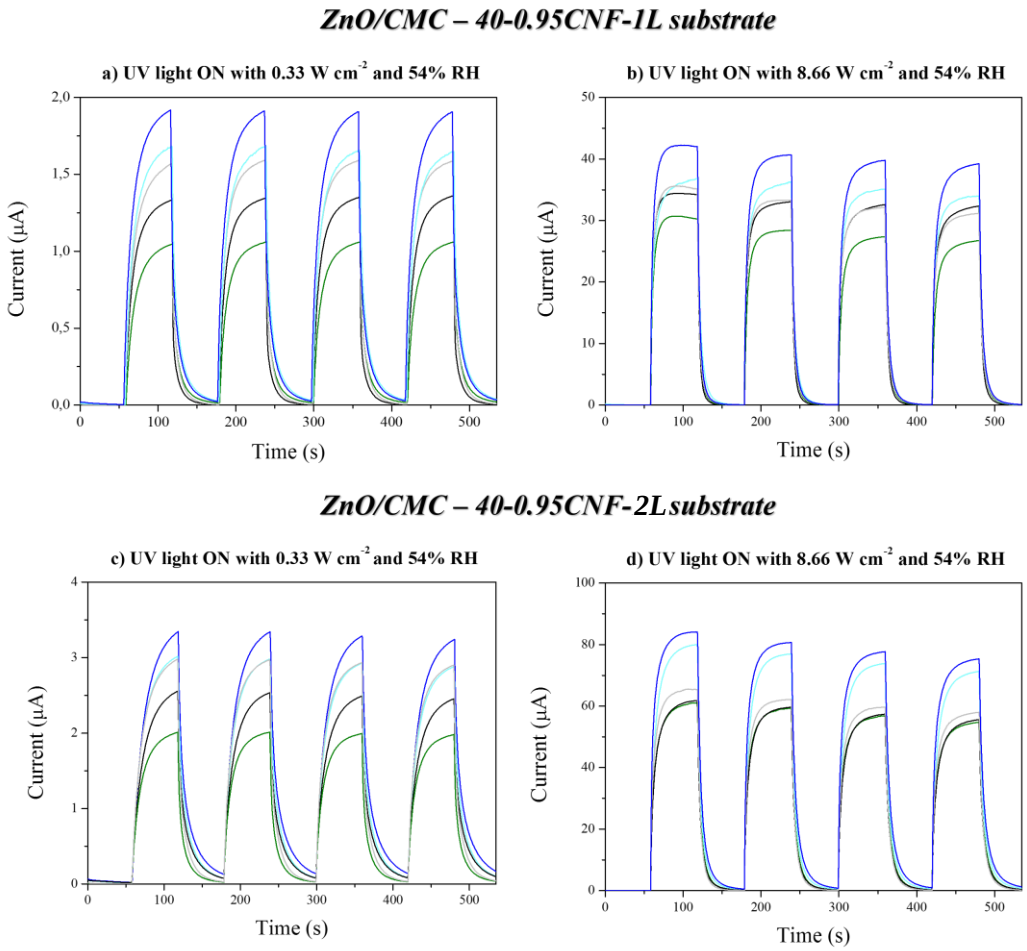

Figure C.5 – Photoresponse curves of five screen-printed ZnO UV sensors on 40-0.95CNF-1L and 40-0.95CNF-2L substrates along four ON/OFF cycles for two UV light intensities.

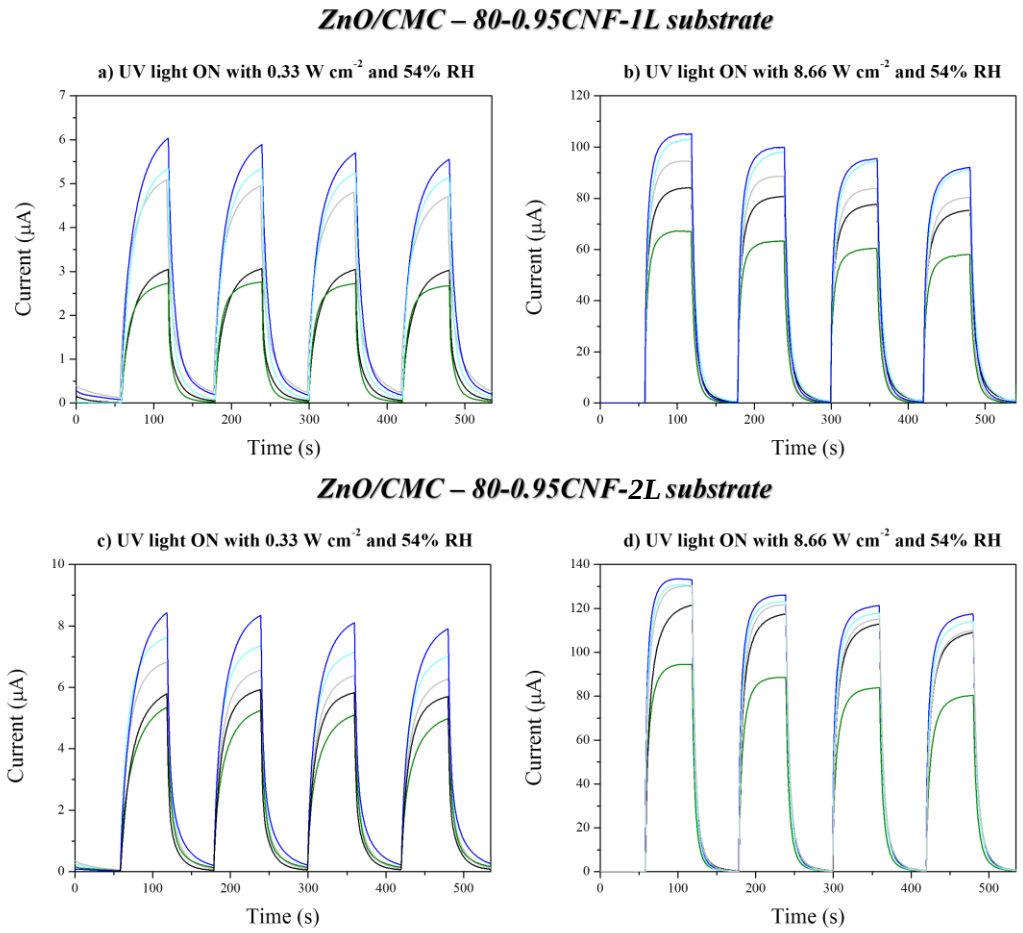

Figure C.6 – Photoresponse curves of five screen-printed ZnO UV sensors on 80-0.95CNF-1L and 80-0.95CNF-2L substrates along four ON/OFF cycles for two UV light intensities.

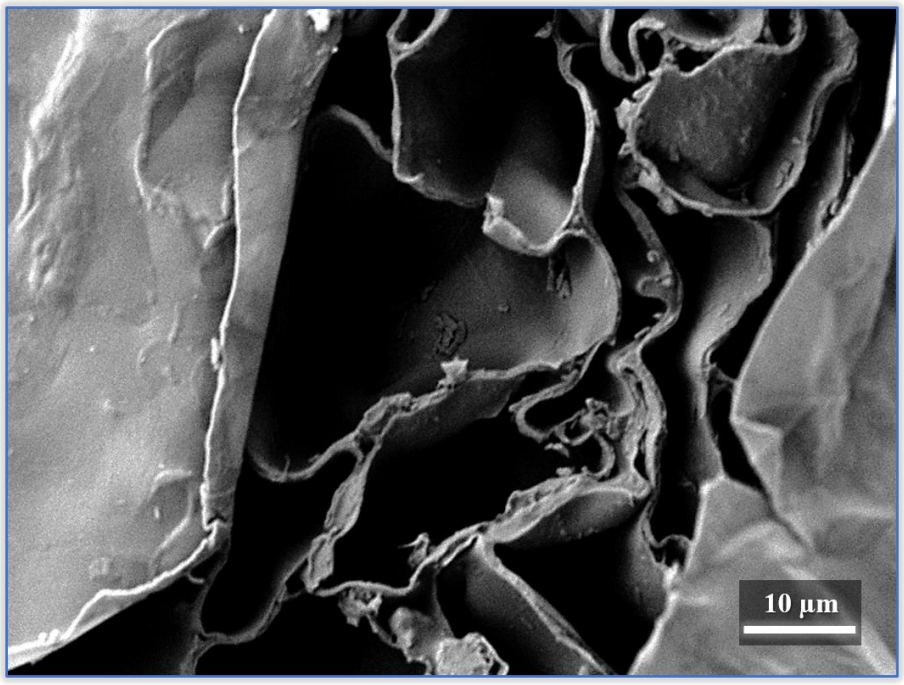

Figure C.7 – Surface CNF membrane crack on the 0.95CNF-M sample.

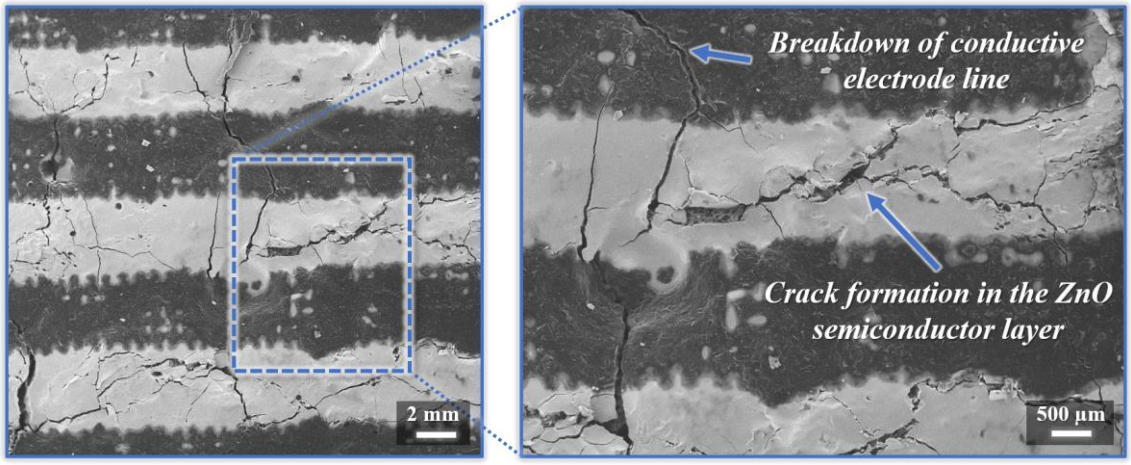

Figure C.8 – SEM images of the UV sensor assembled onto the 40-0.95CNF-1L substrate surface after the 24 hours bending test.